Experimental results on XPW generation

4.1 Introduction

In this chapter I present my experimental results about XPW generation and I compare them with the theory I derived. Before entering the heart of the matter I start giving a brief overview of the different non linear processes that can be used for the contrast cleaning together with an introduction of what where the results about XPW generation when I started my Ph.D.

4.2 Contrast filtering techniques

With the rapid increase of the achievable peak intensity at the output of table top TW laser systems, the temporal contrast of the generated pulses started to attract interest. The European research program named SHARP (Suppression over High dynamic range of ASE at the Rising edge of ultra intense femtosecond pulses) started for the theoretical and experimental investigation of the different solutions for measuring and increasing the temporal contrast in ns regime. This temporal contrast is determined by the ASE, mainly generated in the first, high gain, amplification stage (section 2.2.2).
All the filters that enhance the temporal contrast use a non linear process to exploit the different intensity between the main pulse and the background. A non linear filter is characterized by a relation: $I_{out} = f(I_{in}^n)$, with $n \geq 2$. Considering for example a relative ASE level of 10^{-6} and a second order nonlinear filter, the transmitted intensity is squared and the ASE pedestal is then rejected to a relative intensity of 10^{-12}. The transmitted pulse needs then to be discriminated from the input pulse using for example a difference in wavelength, polarization or phase.
Several nonlinear filters were tested and can be classified by their position in the laser system.

Filters at the beginning or in the middle of the laser system

When the filter is implemented inside the laser system the main non linear effects used are: nonlinear polarization rotation (NER) [9, 11] and cross-polarized wave (XPW) generation [6]. To work correctly these filters have to be seeded with a sufficiently intense, compressed pulse. This means to amplify the pulses in a first CPA to the $> 100\mu J$ level, to clean the pulses after the first compression and then to stretch them again for a further amplification that keeps the ASE constant (using low gain amplifiers).

If the XPW filter is implemented at lower energy, the first CPA can be substituted by an amplification in the fs regime and compensation of the dispersion accumulated during this amplification [1].
Another kind of filter uses a saturable absorber [5] to increase the temporal contrast of the pulse amplified in fs regime without the need to recompress it. This filter can not be applied to repetition rates higher than 10 Hz due to thermal problems.

Filters at the output of the laser system

The second solution is to clean the pulses directly at the the output of the CPA laser. This requires filters with a high transmission efficiency to limit the energy losses in the filtering process. The first non linear process that satisfies this requirement is SHG [13]. Furthermore SHG, dividing by two the wavelength, make it possible to focus the output beam into a smaller focal spot and thereby to maintain the same focused intensity with a lower input energy. The second process is ionization on a dielectric material. In this case the filter is named plasma mirror. Details of this filter will be given in section 7.5. Its drawback is that it is destructive and therefore not well adapted at high repetition rates.

4.3 Historical development of XPW generation

In general, light propagation through nonlinear crystals experiences nonlinear polarization rotation and induced ellipticity (XPW generation). Restricting the analysis to a nonlinear change of the polarization state in non-gyrotropic (without spatial dispersion of the $\chi^{(3)}$ optical nonlinearity) crystals, experiments and theoretical results showed that nonlinear polarization rotation is proportional the imaginary part of the $\chi^{(3)}$ anisotropy ,σ, whereas XPW generation is due to the real part [2, 12, 15, 3, 4]. XPW generation was observed in a range of highly transparent alkali-halide crystals of the m3m group namely NaCl, KBr_2, KCl, LiF, BaF_2. In their transparency range these crystals have $Im[\sigma] = 0$ and $Re[\sigma] \neq 0$.
XPW generation attracted at first interest as a nonlinear process for measuring the magnitude and sign of non linearity tensor's components and its anisotropy in crystals [14]. This non linear process was then extended at the end of the SHARP program as a technique for filtering contrast, in particular through the work of A. Jullien and O. Albert from LOA and N. Minkowski, S. Kourtev and S. Saltiel from the University of Sofia [6].

XPW generation benefits from several advantages in its implementation as a contrast filter: it is a third order nonlinear optical effect degenerate with respect to all frequencies and non degenerate with respect to the polarization vectors of the interacting waves. This means that the generated wave is at the same wavelength as the fundamental and can easily be discriminated using a polarizer with the optical axes orthogonal compared to the input beam. The increase in temporal contrast is defined by the extinction ratio of the polarizers (5-6 orders of magnitude). An impressive measurement of the temporal contrast before and after the XPW filter is shown in Fig. 4.1. Furthermore, as it is a third order nonlinear process, the temporal intensity of the XPW pulse is proportional to the cube of the input pulse intensity. This corresponds, in frequency domain, to a spectral broadening by a factor $\sqrt{3}$ (for Fourier transform Gaussian pulses). This can be very useful for the compensation of gain narrowing in the second CPA. Residual second order spectral phase decreases this broadening and the XPW spectrum becomes $1/\sqrt{3}$ narrower than the input one for large values of the second order phase [10]. This confirms the need to seed the XPW filter with adequately compressed pulses.

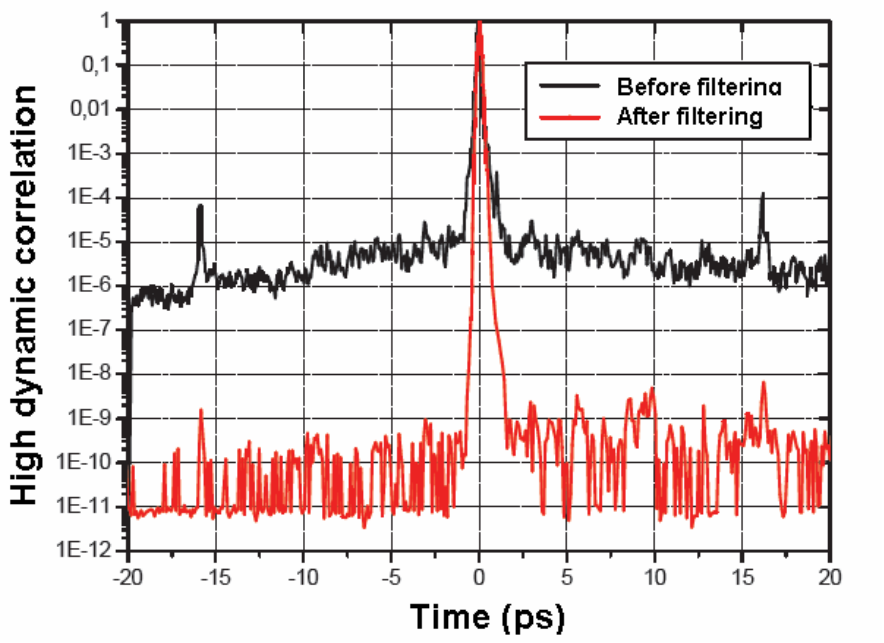

Figure 4.1: Temporal contrast before and after the XPW filter

4.3.1 Design of an efficient XPW generation

Several crystals were tested for efficient XPW generation. A good XPW crystal has to satisfy the following requirements. First it needs to have at least one isotropic plane in linear optics. This corresponds to cubic or tetragonal crystal symmetry. Along this plane the two orthogonally polarized waves propagate with the same group velocity. Crystals with cubic symmetry are preferred because in tetragonal crystals not all planes are isotropic. If the incident wave does not propagating exactly along the z axis of the crystal, a parasitic signal, generated by linear birefringence, is added to the XPW signal. The crystal needs also to be transparent from UV to IR, i.e. with a band-gap larger than 4 eV. This rules out the semiconductors and other

crystal like the Potassium Dihydrogen Phosphate (KDP) or the rutile TiO_2. For cubic crystals XPW generation efficiency depends on the product of the $\chi^{(3)}_{xxxx}$ component, the crystal length L, the input intensity and the anisotropy of $\chi^{(3)}$ -tensor, $\sigma = (\chi^{(3)}_{xxxx} - 3\chi^{(3)}_{xxyy})/\chi^{(3)}_{xxxx}$. Ideally an XPW crystal needs to have a high anisotropy for optimizing XPW generation efficiency and a small non linear index to limit SPM. In Tab. 4.2 I report a list of crystals with $\chi^{(3)}$ anisotropy that can be used for XPW generation. Following the previous considerations, the best crystals for XPW generation are BaF_2, CaF_2 and LiF. In particular, the best crystal for the infrared and visible is the BaF_2, while CaF_2 and LiF are more convenient in the UV (larger band-gap) where two-photon absorption starts to play an important role.

Crystals	Symmetry	Gap (eV)	n	σ
YVO_4	Tetragonal	6	16 [4.3]	+ 0.95 [4.3]
BaF_2	Cubic	9.21 [4.6]	2 [4.7, 4.8]	- 1.2 [4.5, 4.7]
CaF_2	Cubic	9.92 [4.6]	1.3 [4.7]	- 0.6 [4.7]
CdF_2	Cubic	9.54 [4.6]	11.7 [4.7]	+ 0.04 [4.7]
MgF_2	Tetragonal	11.27 [4.6]	0.7 [4.7]	
LiF	Cubic	11.60 [4.6]	0.7 [4.7]	- 0.35 [4.7]
NaCl	Cubic	7.21 [4.6]	4.7 [4.7]	- 0.29 [4.7]
MgO	Cubic	7.77 [4.6]	4.7 [4.7]	- 0.63 [4.7]

Figure 4.2: Table of candidate crystals for XPW generation

The firsts implementations of XPW generation were done using a single [100] (z-cut) crystal cut with a thickness of 1 or 2 mm. In this case the maximum efficiency saturates around 10 %. Increasing the thickness of the crystal does not increase the global efficiency. When the crystal is thicker than $\approx 3mm$, due to self-focusing in the crystal, the threshold for white-light continuum generation is reached before an efficient XPW generation. Furthermore the crystal needs to be thinner than the Rayleigh range of the focusing optics.
From the beginning intense research was made for increasing the efficiency of the process and thus the transmission of the XPW filter. A two-crystal setup was developed that enables reaching an overall efficiency higher than 20 % [8, 7]. The principle of this solution is to use the Kerr lensing in the first crystal in order to refocus the beam into the second crystal. Thanks to the different accumulation of the Gouy phase between the fundamental and the XPW waves by propagation in the space between the crystals, the XPW signals generated in the two crystals can interfere constructively and thus increase the efficiency. This two-crystal solution developed in LOA was patented together with Thales Laser (Patent, French, European and US- # 20060170858).

During my Ph.D I continued the development of the XPW filter with a particular interest in the following goals:

- to further increase the transmission efficiency
- to extend this process to shorter input pulse durations down to the < 10 fs regime.
- to extend this process to shorter wavelengths.

In chapter 3 I demonstrated that the global efficiency depends on the cut of the crystal. In particular it has been predicted theoretically that the [110] cut is the most efficient orientation. This will be confirmed experimentally in the third section of this chapter. Results with a two-crystal scheme to further increase the global efficiency are also presented.
The XPW filter needs to be implemented on compressed pulses. For pulse duration below 30 fs the presence of residual uncompensated higher order spectral phase terms after the first compression can no longer be neglected. It is important to quantify their effect on the XPW spectrum and efficiency. This systematic study is the subject of the fourth section. The extension of this study for sub-10 fs pulses is presented in the fifth section.
The spectrum corresponding to <10 fs pulses can extend over more than one octave and has tails down into the U.V. In all theoretical considerations I assumed a $\chi^{(3)}$ tensor independent of λ. This assumptions is no longer valid on such broad spectral ranges where the photon energy approaches half the band-gap. This motivated the study of the XPW generation in UV presented in the last section.

Bibliography

[1] V. Chvykov, P. Rousseau, S. Reed, G. Kalinchenko, and V. Yanovsky. Generation of 10^{11} contrast 50 TW laser pulses. *Opt. Lett.*, 31(10):1456–1458, 2006.

[2] M. G. Dubenskaya, R. S. Zadoyan, and N. I. Zheludev. Nonlinear polarization spectroscopy in gaas crystals: one- and two-photon resonances, excitonic effects, and the saturation of nonlinear susceptibilities. *J. Opt. Soc. Am. B*, 2(7):1174–1178, 1985.

[3] D. C. Hutchings. Nonlinear-optical activity owing to anisotropy of ultrafast nonlinear refraction in cubic materials. *Opt. Lett.*, 20(15):1607–1609, 1995.

[4] D. C. Hutchings, J. S. Aitchison, and J. M. Arnold. Nonlinear refractive coupling and vector solitons in anisotropic cubic media. *J. Opt. Soc. Am. B*, 14(4):869–879, 1997.

[5] J. Itatani, J. Faure, M. Nantel, G. Mourou, and S. Watanabe. Suppression of the amplified spontaneous emission in chirped-pulse-amplification lasers by clean high-energy seed-pulse injection. *Optics Communications*, 148(1-3):70 – 74, 1998.

[6] A. Jullien, O. Albert, F. Burgy, G. Hamoniaux, J.-P. Rousseau, J.-P. Chambaret, F. Augé-Rochereau, G. Chériaux, J. Etchepare, N. Minkovski, and S. M. Saltiel. 10^{-10} temporal contrast for femtosecond ultraintense lasers by cross-polarized wave generation. *Opt. Lett.*, 30(8):920–922, 2005.

[7] A. Jullien, O. Albert, G. Cheriaux, J. Etchepare, S. Kourtev, N. Minkovski, and S. M. Saltiel. Highly efficient temporal cleaner for femtosecond pulses based on cross-polarized wave generation in a dual crystal scheme. *Appl. Phys. B*, 84:409–414, 2006.

[8] A. Jullien, O. Albert, G. Cheriaux, J. Etchepare, S. Kourtev, N. Minkovski, and S. M. Saltiel. Two crystal arrangement to fight efficiency saturation in cross-polarized wave generation. *Opt. Express*, 14(7):2760–2769, 2006.

[9] A. Jullien, F. Augé-Rochereau, G. Chériaux, J.-P. Chambaret, P. d'Oliveira, T. Auguste, and F. Falcoz. High-efficiency, simple setup for pulse cleaning at the millijoule level by nonlinear induced birefringence. *Opt. Lett.*, 29(18):2184–2186, 2004.

[10] A. Jullien, L. Canova, O. Albert, D. Boschetto, L. Antonucci, Y.-H. Cha, J. P. Rousseau, P. Chaudet, G. Chériaux, J. Etchepare, S. Kourtev, N. Minkovski, and S. M. Saltiel. Spectral broadening and pulse duration reduction during cross-polarized wave generation: influence of the quadratic spectral phase. *Appl. Phys. B*, 87(4):595–601, 2007.

[11] M. P. Kalashnikov, E. Risse, H. Schönnagel, A. Husakou, J. Herrmann, and W. Sandner. Characterization of a nonlinear filter for the front-end of a high contrast double-cpa ti:sapphire laser. *Opt. Express*, 12:5088–5097, 2004.

[12] A.I. Kovrighin, D.V. Yakovlev, B.V. Zhdanov, and N.I. Zheludev. Self-induced optical activity in crystals. *Optics Communications*, 35(1):92 – 95, 1980.

[13] A. Marcinkevičius, R. Tommasini, G. D. Tsakiris, K. J. Witte, E. Gaižauskas, and U. Teubner. Frequency doubling of multi-terawatt femtosecond pulses. *Appl. Phys. B*, 79(5):547–554, 2004.

[14] N. Minkovski, G. I. Petrov, S. M. Saltiel, O. Albert, and J. Etchepare. Nonlinear polarization rotation and orthogonal polarization generation experienced in a single-beam configuration. *J. Opt. Soc. Am. B*, 21(9):1659–1664, 2004.

[15] R. S. Zadoyan, N. I. Zheludev, and L. B. Meysner. Nonlinear polarization spectroscopy of ions interaction potential in alkali halide crystals. *Solid State Communications*, 55(8):713 – 715, 1985.

4.4 Holocut vs z-cut

The theoretical analysis presented in chapter 3 shows that for cubic crystals the holographic cut ensures the highest efficiency with the added advantage that the position of optimal polarization of the fundamental beam is less sensitive to changes in the input intensity. The purpose of this section is:

- to present the experimental results for XPW generation with [011]-cut samples showing an increase in efficiency;
- to show the decreased sensitivity to the orientation of the fundamental beam polarization at high intensity;

The schematic of the set-up with a single BaF_2 situated between crossed polarizers is shown in Fig. 4.3. The derived system of two plane wave equations for the two interacting waves is:

$$\frac{dA(\zeta)}{d\zeta} = i\gamma_1 AAA^* + i\gamma_2 AAB^* + 2i\gamma_2 ABA^* + 2i\gamma_3 ABB^* + i\gamma_3 BBA^* + i\gamma_4 BBB^*, \tag{4.1a}$$

$$\frac{dB(\zeta)}{d\zeta} = i\gamma_5 BBB^* + i\gamma_4 BBA^* + 2i\gamma_4 ABB^* + 2i\gamma_3 ABA^* + i\gamma_3 AAB^* + i\gamma_2 AAA^*. \tag{4.1b}$$

where A and B denote the amplitudes of the fundamental and cross-polarized waves, respectively. The γ coefficients derived for both cuts are summarized in Tab. 4.5. The last line in the table I gives the orientations of input polarization β_{zero} for which the XPW signal is zero. These angles, derived from $\gamma_2(\beta) = 0$, are different for the two cuts and this can be used to test the correct orientation of the [011]-cut sample. The NLC used in the experiments are 2

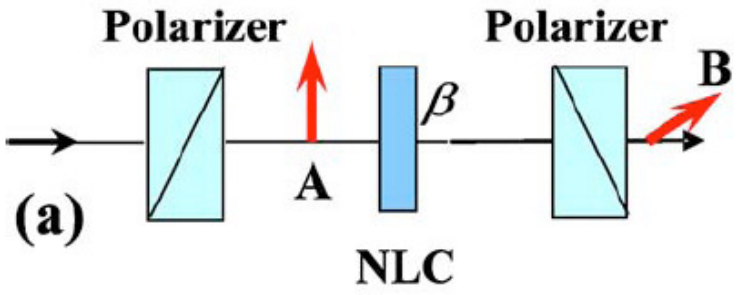

Figure 4.3: Schematic of the XPW generation experiment

mm thick z-cut and [011]-cut BaF_2 crystals. The BaF_2 sample is placed between two calcite Glan polarizers with an extinction ratio better than 4 orders of magnitude. Both the BaF_2

samples and the polarizers are un-coated. The β-dependence measurements were performed with the second harmonic of a Colliding Pulse Mode Locked (CPM) dye-laser (620 nm, 100 fs, 10 Hz-Salle Rose). The pulses with an energy up to 20 μJ were focused with a $f = 500$ mm lens into the NLC. Fig. 4.4 shows the experimental β dependence of XPW generation in the [011]-cut sample. The theoretical curves (lines) for Gaussian/Gaussian shapes for spatial/temporal modulation of the fundamental radiation are obtained by numerically solving the system 3.9. The agreement with experiment is good. The angles β_{zero} for which the XPW signal is minimal correspond to the values listed in Tab. 4.5. As predicted, the two main β position maxima for the holographic cut are insensitive to changes in input energy.

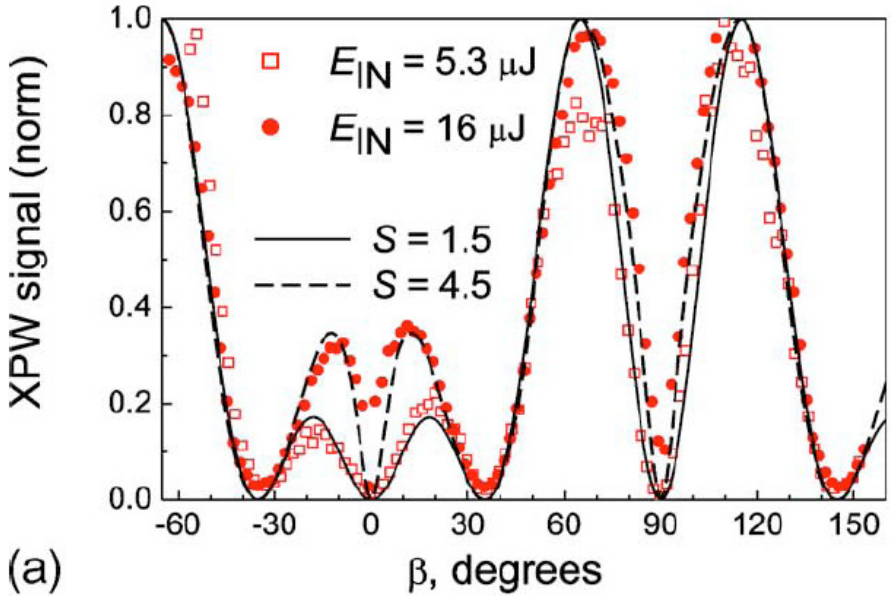

Figure 4.4: XPW signal as a function of angle β for [011] orientation for two different input energies. The lines are theoretical curves.

XPW generation efficiency measurements were done with a commercial femtosecond laser (Femtopower PRO CEP, Femtolasers GmbH) delivering up to 1 mJ, 30 fs pulses at 1 KHz. The fundamental beam spatial shape is very close to Gaussian as shown in the inset of Fig. 4.6. The pulse-to-pulse stability of the laser used in the experiment is below 1% ensuring a very small error (3%) in the efficiency measurements. Measured conversion efficiencies (without corrections for losses) for experiments with a single BaF_2 crystal are shown in Fig. 4.6. The pulses are focused with a $f = 500$ mm lens into the NLC. The efficiency with [011]-cut sample saturates at 11.4%. This value can be compared with the maximum efficiency of 10% measured with a single crystal (Fig. 4.6). Accounting for losses of the output Glan and the NLC, an internal efficiency of 15% is obtained. This efficiency saturates earlier than in the simulation because in the theoretical model we neglect diffraction and self-focusing. It is very important to note that the efficiency curve for the [001]-cut (circles) in Fig. 4.6 was obtained with reoptimization of angle β, while for experiment with the [011]-cut (squares) such a reoptimization was not necessary as predicted by the model.

	z-cut	Holographic cut
γ_1	$\gamma_0[1-(\sigma/2)\sin^2(2\beta)]$	$\gamma_0[D-(\sigma/4)\cos 2\beta]$
γ_2	$-(\gamma_0\sigma/2)\sin 2\beta\cos 2\beta$	$-(\gamma_0\sigma/8)\sin 2\beta(3\cos 2\beta-1)$
γ_3	$(\gamma_0/3)(4-\sigma)-\gamma_1$	$(\gamma_0/3)[D-(3\sigma/4)\cos 4\beta]$
γ_4	$-\gamma_2$	$(\gamma_0\sigma/8)\sin 2\beta(3\cos 2\beta+1)$
γ_5	γ_1	$\gamma_0[D+(\sigma/4)\cos 2\beta]$
β_{zero}	0°; 45°; 90°; 135°; 180°	0°; 35.3°; 90°; 144.7°; 180°

Figure 4.5: Nonlinear coupling coefficients both for z-cut and holographic cut. D stands for: $1+(3\sigma/16)cos4\beta-7\sigma/16$, $\gamma_0=6\pi\chi^{(3)}_{xxxx}/8n\lambda$

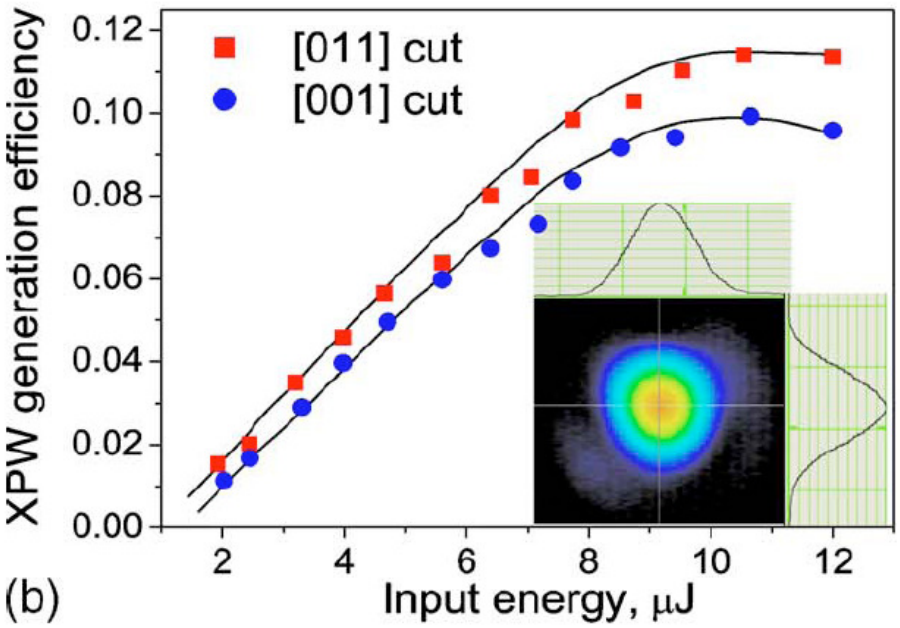

Figure 4.6: XPW generation efficiencies for the two cuts. Insets:input fundamental beam spatial shape.

As XPW filtering is useful at higher energy in a double CPA scheme, we also tested a two crystals scheme [1, 8] for XPW generation using two holographic cut BaF_2 crystals. The fundamental beam with a diameter of 7 mm was focused with a $f = 5$ m lens. The two crystals were set ≈ 50 cm apart, in accordance with the experimental dependence pointed out in [10]. The obtained XPW energy and efficiency are shown Fig. 4.7. The output spectrum has a near Gaussian shape with 80 nm FWHM (for an input width of 50 nm). The maximum obtained

efficiency of 29 % for a 190 μJ input pulse energy yields a 55 μJ XPW pulse energy. It is the highest XPW energy efficiency recorded so far with this kind of set up. This value is in fact 1.3 times higher than the previously published values obtained with z-cut crystals (see [8, ?, 9]) which is in accordance with the prediction of the model. Considering the output pulse shortening obtained via XPW generation this result corresponds to a 50% intensity conversion from one polarization to another. Highest efficiencies are obtained for an input energy just below the continuum generation threshold.

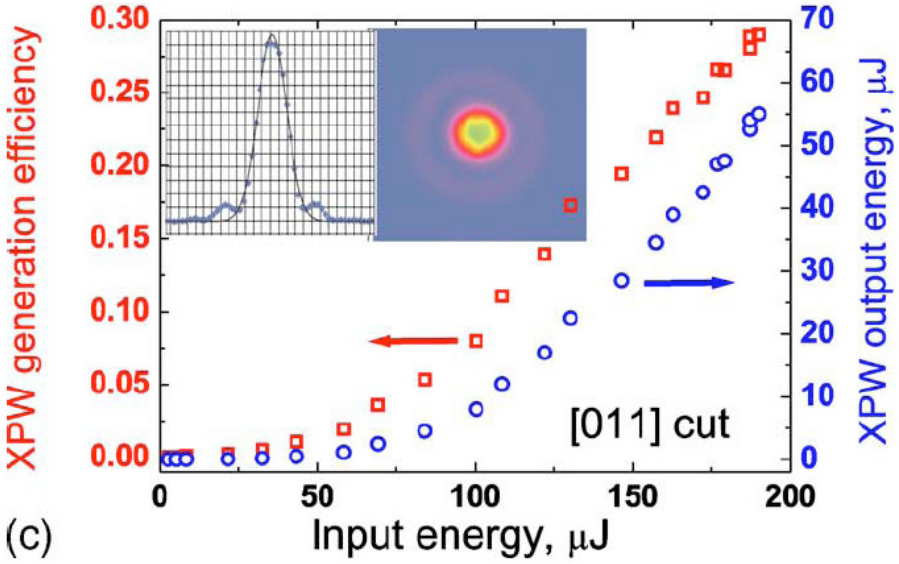

Figure 4.7: XPW generation energy (circle) and efficiency (square) for two crystal scheme with two holografic cut BaF_2 crystals. Insets: output XPW spatial shape

4.5 Conclusions

Record efficiencies for XPW generation using holographic ([011])-cut BaF_2 crystals (and Gaussian beams) have been demonstrated thereby confirming the theoretical predictions. I also demonstrated that when [011]-cut crystals are used for XPW generation, intensity dependent β compensation of the phase mismatch is not required. This feature makes the holographic cut easier to use for all XPW generation applications.

Bibliography

[1] A. Jullien, O. Albert, G. Cheriaux, J. Etchepare, S. Kourtev, N. Minkovski, S.M.Saltiel, Appl. Phys. B **84**, 409 (2006).

[2] V. Chvykov, P. Rousseau, S. Reed, G. Kalinchenko, and V. Yanovsky. Generation of 10^{11} contrast 50 TW laser pulses. *Opt. Lett.* **31**, 1456 (2006)

[3] N. Minkovski, G. I. Petrov, S. M. Saltiel, O. Albert, and J. Etchepare. Nonlinear polarization rotation and orthogonal polarization generation experienced in a single-beam configuration. *J. Opt. Soc. Am. B* **21**, 1659 (2004)

[4] Yu. P. Svirko and N. I. Zheludev, *Polarization of Light in Nonlinear Optics* (Wiley, New York, 1998).

[5] N.Minkovski, S.Saltiel, G. Petrov, O. Albert, J. Etchepare, Opt. Lett. **27**, 2025 (2002).

[6] M. Dabbicco, A. M. Fox, G. von Plessen, J. F. Ryan, Phys. Rev. B **53**, 4479 (1996).

[7] V. M. Gordienko, P. M. Mikheev, V. S. Syrtsov, Bulletin RAS: Physics **71**, 122 (2007).

[8] A. Jullien, O. Albert, G. Cheriaux, J. Etchepare, S. Kourtev, N. Minkovski, S. M. Saltiel , Opt. Express **14** , 2760 (2006).

[9] A. Cotel, A. Jullien, N. Forget, O. Albert, G. Ch´eriaux, C.L. Blanc, Appl. Phys. B **83**, 7 (2006).

[10] O. Albert, A. Jullien, J. Etchepare, S. Kourtev, N. Minkovski, S. M. Saltiel, Opt. Lett. **31**, 2990 (2006).

4.6 Effect of the spectral phase on XPW generation

In this section I present the first comprehensive study of the role of spectral phase on XPW generation using sub-30 fs laser pulses. For durations comprised between 30 and 10 fs the presence of residual uncompensated higher order spectral phase terms after the first compression can no longer be neglected and it is important to quantify their effect on the XPW spectrum and efficiency. For those short pulses, compression is achieved after measurement of the spectral phase with a SPIDER or a FROG. For a 30 fs pulse measurement precision is on the order of 100 fs^2 and 10000 fs^3 for the second and third order of the spectral phase [12, 13, 14]. As it will be demonstrated, within this range of residual spectral phase the XPW output spectrum can be significantly modified, especially with residual higher order spectral phase. I will also derive the maximum acceptable value of residual phase for a given initial pulse duration in order to efficiently drive the XPW process for pulse shortening and contrast improvement.

The XPW experimental setup is shown in Fig. 4.8. We use a commercial femtosecond laser (Femtolasers GmbH) delivering 1 mJ, 30 fs pulses at 1 kHz. The spectral phase of the compressed pulses was measured with an homemade SPIDER [20] and corrected using an acousto-optical programmable dispersive filter (AOPDF, Dazzler™ [21]) inserted into the chirped pulse amplifier. By doing so we have noticed that we removed $\varphi^{(4)} \sim -2.10^6\, fs^4$ and $\varphi^{(5)} \sim 50.10^6\, fs^5$. Furthermore, in order to test the effect of remaining spectral phase higher order terms, we can cancel the Dazzler correction and make experiment with known $\varphi^{(4)}$ and $\varphi^{(5)}$ values.

To study experimentally the effect of the spectral phase on the XPW process, I used a second AOPDF (25 mm TeO_2 crystal) as a versatile and precise way to tune the spectral phase on demand. This AOPDF is placed between the laser and the XPW setup. To avoid damaging the AOPDF, only 1 μJ is used from the total laser energy for our experiments. The diffracted output of the AOPDF is focused by a 40 mm focal length achromatic lens into a 1 mm thick BaF_2 crystal, the XPW beam is selected through a polarizer and focused onto the entrance slit of a spectrometer (Avantes). Both AODPF and spectrometer were synchronized with the laser pulses. The spectral phase from the laser was considered flat, except for the cases when we deliberately introduce the known higher order residual phase. The AOPDF was first set to compensate both its own dispersion and that of the focusing lens in a static way. We then use the AOPDF to add to the optical pulse some user-defined spectral phase. In the experiments presented we added the following spectral phases:

$$\delta\varphi(\omega) = \varphi^{(2)} (\omega - \omega_0)^2 /2 + \varphi^{(3)} (\omega - \omega_0)^3 /6 \tag{4.2}$$

Both coefficients $\varphi^{(2)}$ and $\varphi^{(3)}$ were automatically scanned between -2000 fs^2 and +2000 fs^2 for $\varphi^{(2)}$ (32 points) and between -60000 fs^3 and +60000 fs^3 for $\varphi^{(3)}$ (16 points). For each $\delta\varphi(\omega)$, a different acoustic wave was loaded into the AOPDF generator and the XPW spectrum was recorded and processed. With this setup, a systematic experimental analysis of the effect of cubic spectral phase on the XPW spectrum and efficiency was made possible.

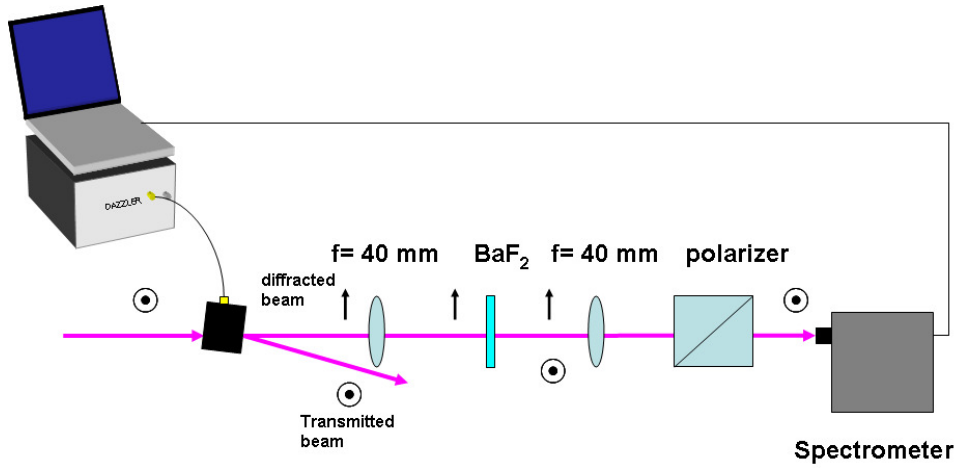

Figure 4.8: Experimental setup.

4.6.1 XPW efficiency

The first dependence considered is the influence of spectral phase on XPW efficiency. As the input energy is constant, the XPW efficiency is proportional to the XPW output energy. Therefore, the XPW efficiency is obtained by integrating every acquired XPW spectrum over the whole spectral range. Fig. 4.9 shows the obtained experimental efficiency map that should be compared with the theoretical map shown in Fig. 3.15. In both cases there is a global maximum of the efficiency corresponding to $\varphi^{(2)} = \varphi^{(3)} = 0$. This is due to the fact that XPW (as all nonlinear effects) is highly sensitive to peak intensity and the highest peak intensity is obtained for a pulse with a flat spectral phase. Fig. 4.10 presents cross sections of this map for $\varphi^{(3)} = 0\, fs^3$ and for $\varphi^{(2)} = 0\, fs^2$. The theoretical curves are obtained from the same cross sections of Fig. 3.15. As predicted, the efficiency decreases with second order phase with a Lorentzian dependence. In particular the experimental $\varphi^{(2)}_{\mathrm{cr,Energy}} = +350\, fs^2$ corresponds to the theoretical one. As a reminder $\varphi^{(2)}_{\mathrm{cr,Energy}}$ is the value of the second order dispersion for which the XPW efficiency is equal to half of the maximum conversion efficiency. The variation of the XPW efficiency with third order spectral phase fits also with the numerical calculation. The difference between the two curves is due to the imprecision of the measurement and correction from high order spectral phase terms.

In the case of a laser pulse with a residual spectral phase ($\varphi^{(4)} \sim -2.10^6\, fs^4$ and $\varphi^{(5)} \sim 50.10^6\, fs^5$) the efficiency dependence on $\varphi^{(2)}$ and $\varphi^{(3)}$ becomes asymmetric (Fig. 4.11.a). This behavior can be reproduced numerically (Fig. 4.11.b). To center the map, both coefficients $\varphi^{(2)}$ and $\varphi^{(3)}$ were scanned between -1500 fs^2 and +4000 fs^2 for $\varphi^{(2)}$ and between -80000 fs^3 and +80000 fs^3 for $\varphi^{(3)}$. The asymmetry can be explained intuitively. When $\varphi^{(2)}$ reaches a value corresponding to the opposite of the residual $\varphi^{(4)}$ value, the effect of both phase terms mutually

compensate, yielding better efficiency. When $\varphi^{(2)}$ and $\varphi^{(4)}$ have the same sign the effect of both phase terms sum up. This gives the vertical asymmetry in Fig. 4.11.a,b. The horizontal asymmetry is due to the same combination of effects between $\varphi^{(3)}$ and $\varphi^{(5)}$. Furthermore, maximum efficiency (which is less than in the case of a perfect flat phase) is reached at a non-zero [$\varphi^{(2)}$,$\varphi^{(3)}$] where the input spectral phase is the flattest.

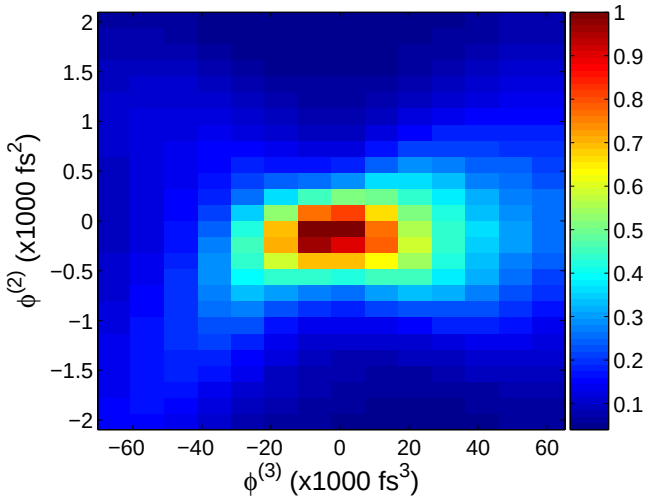

Figure 4.9: Experimental 2D plot of the normalized XPW efficiency versus $\varphi^{(2)}$ and $\varphi^{(3)}$ after compensation of the higher order spectral phase terms. The maximum signal corresponds to an XPW efficiency of 5%.

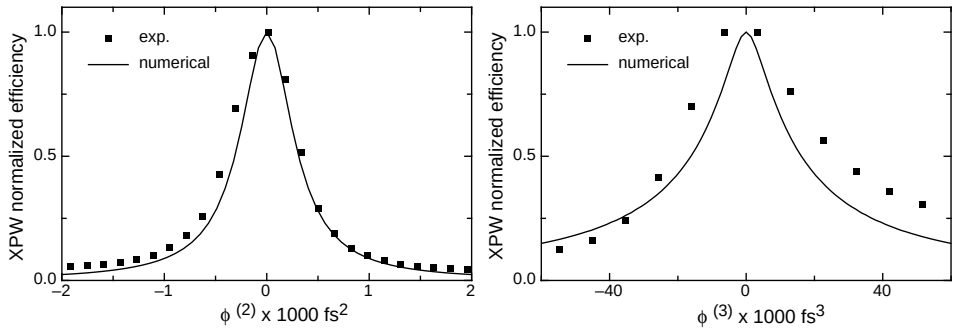

Figure 4.10: Left: normalized experimental (points), (dashed line) and theoretical Lorentzian (solid line) XPW efficiency as a function of $\varphi^{(2)}$ for $\varphi^{(3)} = 0$. Right: normalized experimental points and theoretical (solid line) XPW efficiency as a function of $\varphi^{(3)}$ for $\varphi^{(2)} = 0$

4.6.2 Spectral width

Fig. 4.12 shows the map displaying the spectral width of the previously acquired spectra. These data have been obtained with a laser pulse uncorrected for higher order spectral phase terms, so the theoretical curve in Fig. 4.12 is calculated using $\varphi^{(4)} \sim -2.10^6\, fs^4$ and $\varphi^{(5)} \sim 50.10^6\, fs^5$.

It can be noticed again that there is a global maximum of the spectral width when the total spectral phase is almost flat since both the efficiency and the spectral width reach their

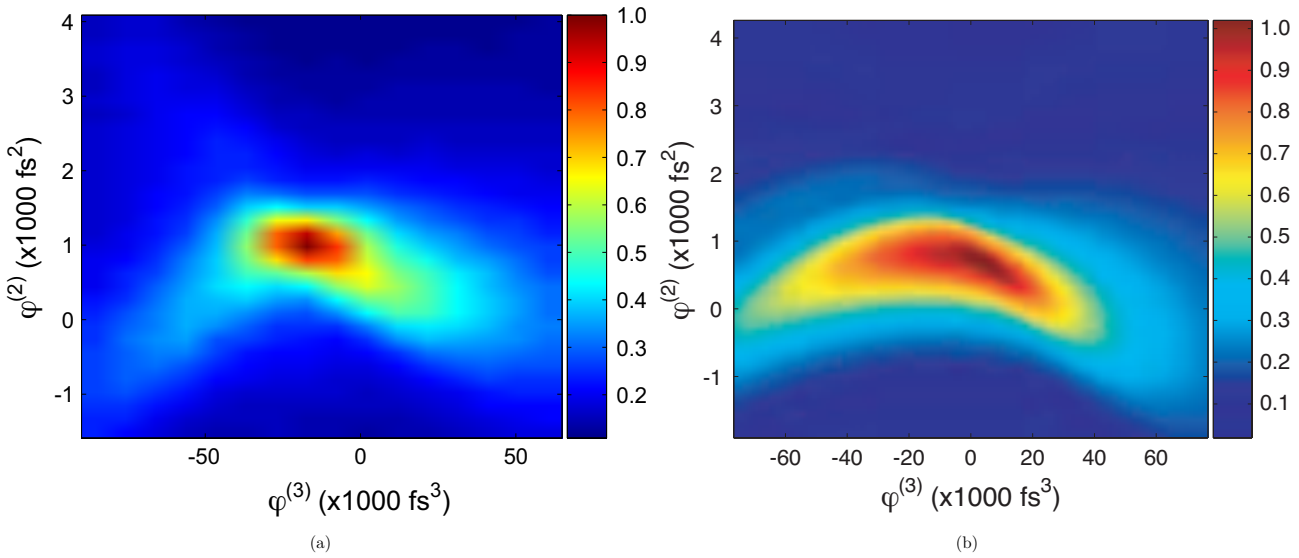

Figure 4.11: Experimental (a) and theoretical (b) 2D plot of the normalized XPW efficiency versus $\varphi^{(2)}$ and $\varphi^{(3)}$ with known residual $\varphi^{(4)}$ and $\varphi^{(5)}$.

maximum for the same ($\varphi^{(2)}$,$\varphi^{(3)}$). The asymmetry of the maps 4.12 is very similar to that already discussed for the efficiency map. As previously presented this can be explained by the presence of residual higher order spectral phase. These experiments confirm the sensitivity of the XPW spectral width to the initial spectral phase. In particular there is spectral broadening of the XPW spectrum compared to the fundamental spectrum for a limited range of $\varphi^{(2)}$,$\varphi^{(3)}$. These values for $\varphi^{(2)}_{\mathrm{cr,Width}}$ and $\varphi^{(3)}_{\mathrm{cr,Width}}$ derived experimentally are comparable to the numerical prediction.

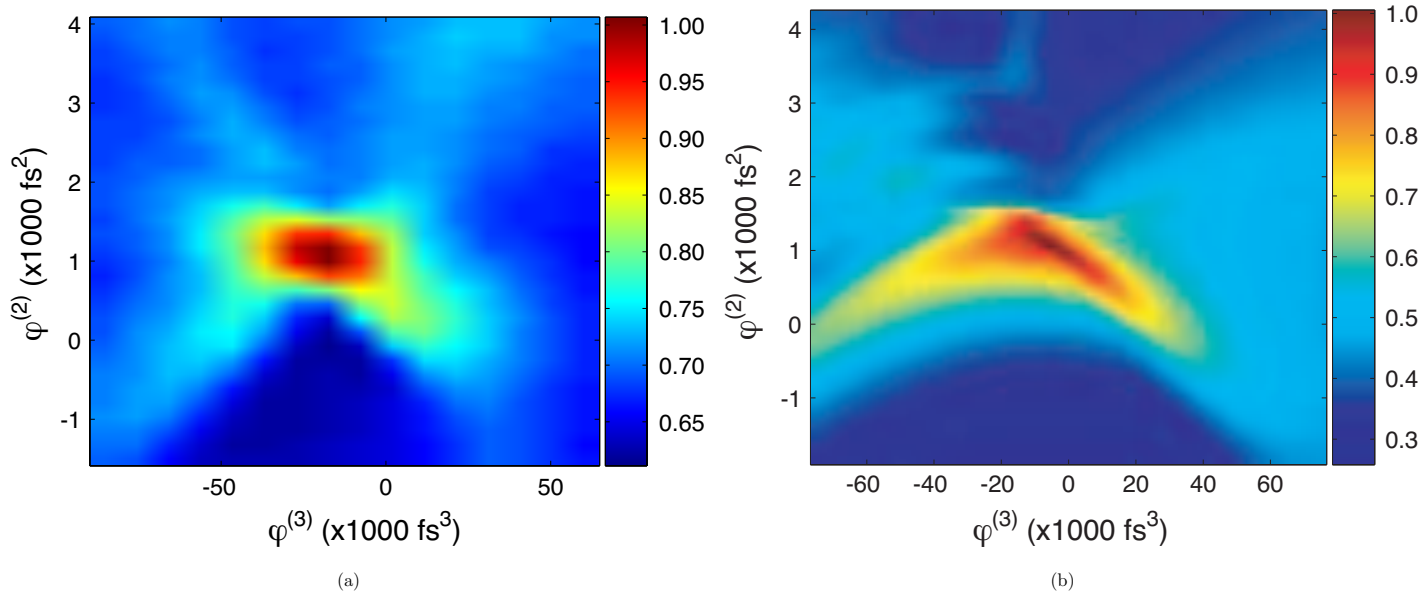

Figure 4.12: Experimental (a) and theoretical (b) 2D plot of the XPW pulse spectral width versus $\varphi^{(2)}$ and $\varphi^{(3)}$. The spectral width values are normalized to the maximum (best compression of the input pulse) of the 2D plot.

4.6.3 Spectral shift

The last parameter considered is the shift of the center of mass of the XPW spectrum. Fig. 4.13(a) shows the center of mass shift of the XPW spectrum as a function of [$\varphi^{(2)}$, $\varphi^{(3)}$] in the case of uncompensated higher order spectral phase terms. This map is in agreement with the hyperbolic parabola derived in the case of a pure $\varphi^{(2)}$, $\varphi^{(3)}$ scan. The analytical model derived in the theoretical section shows that for a residual $\varphi^{(2)}$ and $\varphi^{(3)}$ the spectrum becomes asymmetric. It also indicates that for a fixed and large value of $\varphi^{(3)}$, the center of mass shifts linearly with $\varphi^{(2)}$. The sign of the slope of this curve depends on the sign of $\varphi^{(3)}$. This is confirmed by experiments (Fig. 4.14) in the zone where this approximation is valid. It can also be noticed that this linear shift does not continue indefinitely for larger values of $\varphi^{(2)}$. By changing the input cubic spectral phase a global shift of the center of mass is obtained which is at maximum 1/3 of the spectral bandwidth. The shift of the XPW spectral center of mass function of $\varphi^{(2)}$ for two symmetrical values of $\varphi^{(3)}$ is not perfectly symmetric (for example Fig. 4.14) due to the higher order residual phase terms.

Comparing Fig. 3.16(a) and fig. 4.13(a) around the zone of optimum input pulse compression (center of the map, saddle point) it is visible that the experimental map has an additional shift towards shorter wavelengths (the color is light blue) compared to the theoretical one (where the color is yellow (Fig. 3.16a)). Simulations with the residual $\varphi^{(4)}$ and $\varphi^{(5)}$ spectral phase mentioned previously, reproduce this spectral shift as shown in Fig. 4.13(b). The center of mass of the XPW spectrum is visibly influenced by the higher order spectral phase also near $\varphi^{(2)} = \varphi^{(3)} = 0$ with a shift towards shorter wavelengths when $\varphi^{(4)}$ and $\varphi^{(5)}$ are of opposite sign and towards longer wavelengths when they are of the same sign. Therefore, higher order spectral phase terms have an influence on the XPW signal for any values of [$\varphi^{(2)}$,$\varphi^{(3)}$]. They shift the central wavelength, and influence the XPW efficiency and spectral width for higher values of $\varphi^{(2)}$ and $\varphi^{(3)}$.

4.7 Practical experimental conditions for XPW generation

This systematic theoretical and experimental analysis gives a general idea of the role of the spectral phase on the XPW nonlinear process. In particular it is possible to extract experimentally the maximum tolerable values of residual spectral phase for an input pulse of 30 fs. I have demonstrated that it is fundamental to compensate at least a pure second order spectral phase to a residual value lower than $\pm 325\, fs^2$ and the pure third order phase to a residual value lower than $\pm 17500\, fs^3$ to obtain half of the maximum XPW efficiency. In this range the XPW spectrum is broadened and the center of mass is shifted at maximum by 4 nm compared to the fundamental which is perfectly adapted for amplification in a Ti:Sa amplifier. These values of spectral phase are slightly increased ($\pm 500\, fs^2$and $\pm 25000\, fs^3$) when residual higher

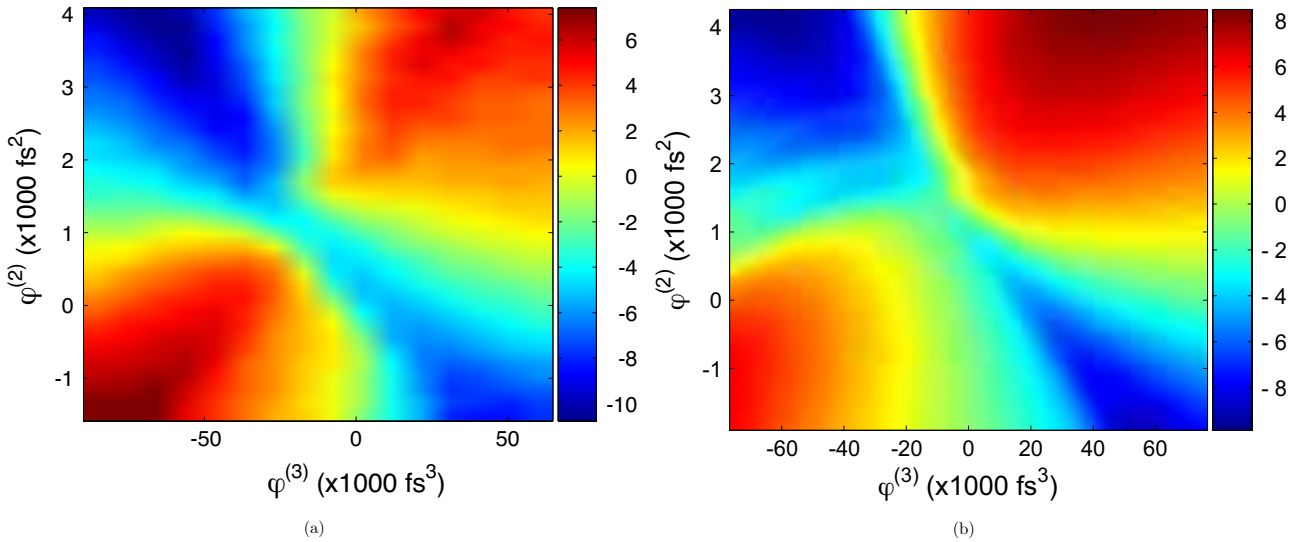

Figure 4.13: Experimental (a) and theoretical (b) 2D plot of XPW spectra center of mass shift (in nm) versus $\varphi^{(2)}$ and $\varphi^{(3)}$ with known residual $\varphi^{(4)}$ and $\varphi^{(5)}$.

order spectral phase terms are present. This can be understood as, for a spectral phase with some residual higher order terms, the XPW signal is lower than the one obtained for a perfectly compressed pulse. Those spectral phase higher order terms can be compensated by a wide combination of second and third order terms. Therefore, it broadens the region for which the XPW efficiency is kept above half of the maximum efficiency. In this case there is a shift of the center of mass even with perfect compensation of $\varphi^{(2)}$ and $\varphi^{(3)}$ terms. These values agree with the numerical simulations.

For a given stretcher compressor system, those $\varphi^{(2)}$ and $\varphi^{(3)}$ values can be correlated to a range of acceptable grating spacing variation and a range of incident angle variations that preserve an efficient XPW generation. Those ranges can also be seen as the degree of precision needed for the given stretcher compressor system to allow an efficient XPW generation.

As this range of $\varphi^{(2)}$ and $\varphi^{(3)}$ values for efficient XPW generation is of the same order of magnitude as the measurement precision obtained with a FROG or a SPIDER, the best approach is to tune the stretcher compressor system to the optimum and then tune the compressor slightly to optimize the XPW generation efficiency without spectral shift.

We can next generalize this analysis to shorter input pulse durations. This is important as it allows to know in general, when the input pulse can be defined as "Fourier limited" with respect to the XPW generation process. Fig. 4.15 (a) shows the [$\varphi^{(2)}$,$\varphi^{(3)}$] area for which efficiency is reduced by less than half calculated for 30, 20 and 10 fs pulses. The elongated peanut shape of these areas is due to partial compensation between $\varphi^{(2)}$ and $\varphi^{(3)}$ which induces a partially flat

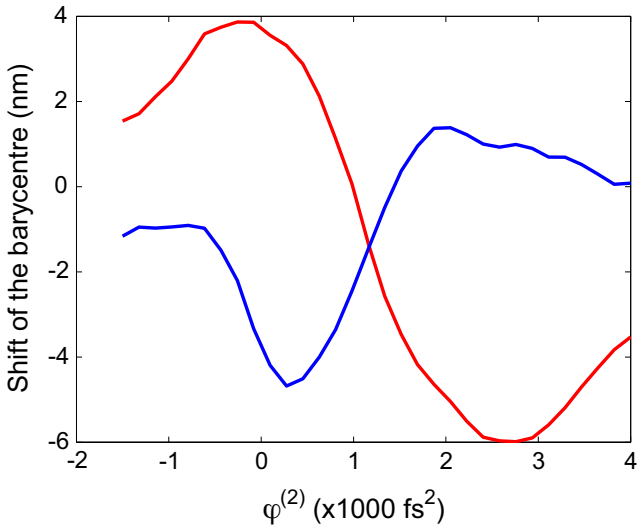

Figure 4.14: Shift of the XPW spectra center of mass as a function of $\varphi^{(2)}$ for $\varphi^{(3)} = -20000\, fs^3$(red) and $\varphi^{(3)} = +20000\, fs^3$(blue). These curves are obtained from cross-sections of Fig. 4.13(a)

spectral phase preventing excessive stretching of the pulse. Higher order phase terms break the symmetry of these plots and can also be evaluated theoretically. This figure confirms how fast the acceptable area decreases decreasing input pulses duration.

As demonstrated in [10] the chirp of the generated XPW pulse is reduced up to nine times compared to the incident pulse chirp. This improvement is less increasing input chirp and reaches a value equal to the input one for large values of input chirp. This behavior can be extended for higher order phase terms as has been done for second order nonlinearities [19]. Therefore we can predict that the spectral phase of the XPW pulse is flattened for the values of $\varphi^{(2)}$ and $\varphi^{(3)}$ yielding good XPW efficiency (i.e. in the area defined by Fig. 4.15 (a)). This area is the one typically used for contrast improvement with XPW, and corresponds to the area where XPW also improves the coherent contrast of the pulse [4]. Outside this area the XPW spectral phase corresponds to the input pulse spectral phase.

Fig. 4.15 (b) shows the [$\varphi^{(2)}$,$\varphi^{(3)}$] area that preserves the initial spectral width of the laser for the same input pulse durations. This area is broader than the area for efficient XPW generation (Fig. 4.15 a). XPW spectra generated for a couple [$\varphi^{(2)}$,$\varphi^{(3)}$] at the border of this area are modulated by the coupling of the input pulse spectral phase to the spectral amplitude of the XPW through the nonlinear process. This effect could allow approximate spectral tailoring in some coherent control experiments. This is emphasized by the fact that the main feature of the tailoring using the spectral phase is a controllable central wavelength shift.

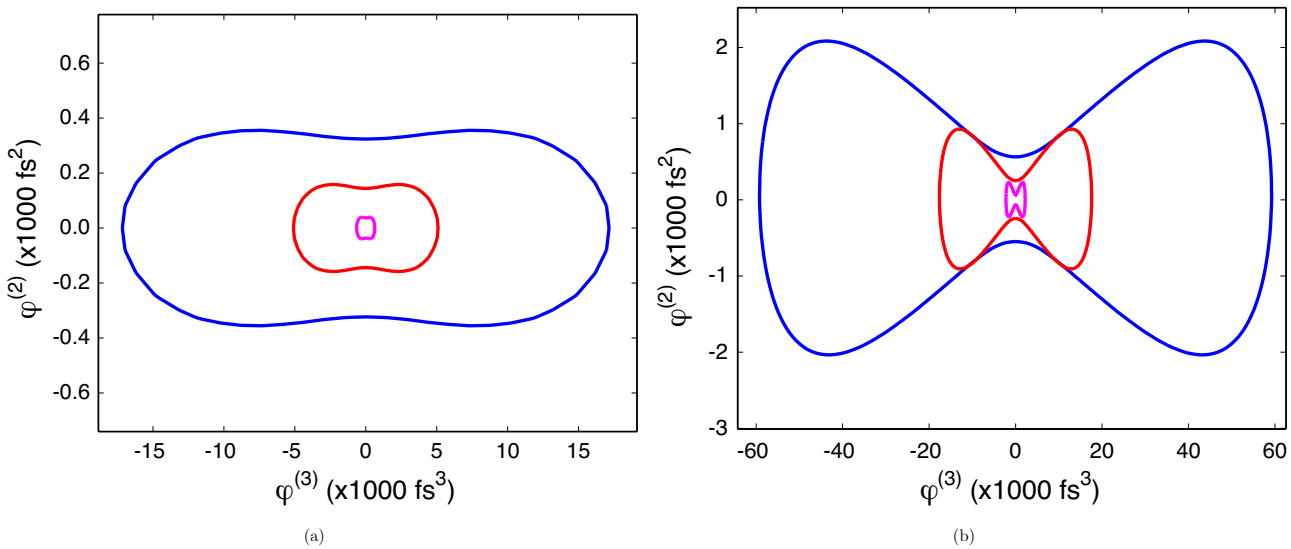

Figure 4.15: (a) Contour line representing the maximum values of $\varphi^{(2)}$and $\varphi^{(3)}$ to obtain half of the maximum XPW efficiency for respectively 30 fs (blue), 20 fs (red) and 10 fs (purple) input pulse duration. (b) Contour line representing the maximum values of $\varphi^{(2)}$and $\varphi^{(3)}$ to obtain $\Delta\lambda_{XPW} = \Delta\lambda_{laser}$ for respectively 30 fs (blue), 20 fs (red) and 10 fs (purple) input pulse duration (b). The range of both axis is different for the two figures i.e. the areas on (a) are broader that the corresponding areas on the (b).

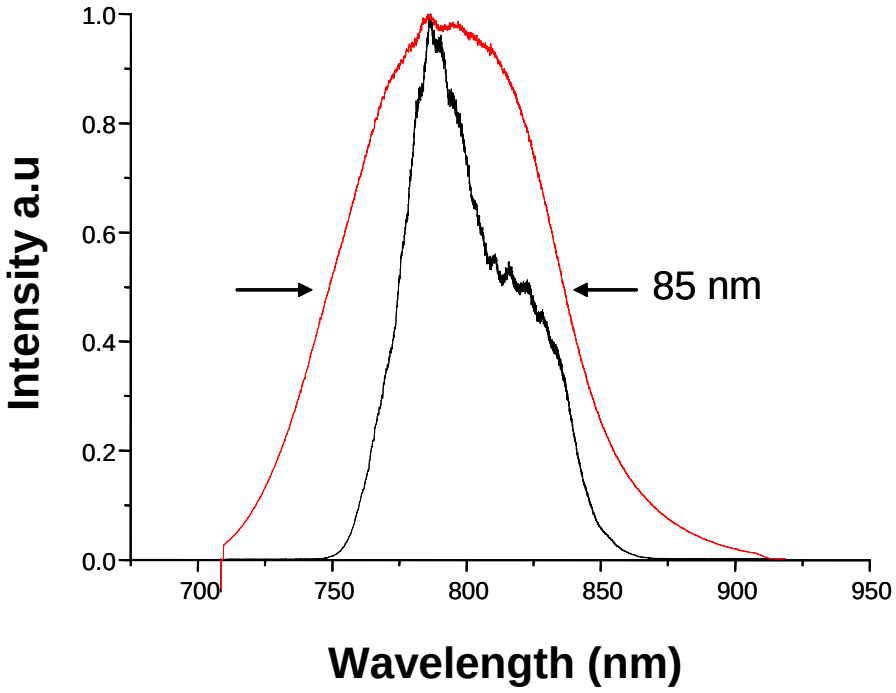

Figure 4.16: Spectrum of the input pulse (black) and of the XPW generated pulse (red). The XPW spectrum is Gaussian, broadened by a factor $\sqrt{3}$ and centered at the same wavelength than the input pulse giving a FWHM of about 85 nm. The input pulse is optimally compressed with a Dazzler.

4.8 Conclusions

In this section I demonstrate the importance of controlling the spectral phase of the input pulse for a correct generation of Cross-Polarized Wave with sub-30 fs pulses and how to optimize the pulse compression after the first CPA directly with the nonlinear effect of the XPW filter. With this control the XPW filter maintains all its benefits (increasing of ns and ps temporal contrast, spectral broadening) for pulses as short as 10 fs.

Fig. 4.16 shows a 85 nm XPW spectrum obtained from a 47 nm input spectrum. The compression of the input pulse was optimized with the Dazzler to obtain a transform limited pulse. The XPW spectrum is Gaussian, broadened by a factor $\sqrt{3}$ and centered at the same wavelength as the input pulse. Following the discussion presented in this section this demonstrates the optimal compression of the input beam. It is important to notice that, due to the spectral filtering, the XPW spectrum is Gaussian even with a modulated input spectrum. This feature can be very useful for sub-10 fs and is discussed in the next section.

Bibliography

[1] N. Minkovski, G. I. Petrov, S. M. Saltiel, O. Albert, and J. Etchepare. Nonlinear polarization rotation and orthogonal polarization generation experienced in a single-beam configuration. *J. Opt. Soc. Am. B* **21**, 1659 (2004)

[2] A. Jullien, O. Albert, F. Burgy, G. Hamoniaux, J.-P. Rousseau, J.-P. Chambaret, F. Augé-Rochereau, G. Chériaux, J. Etchepare, N. Minkovski, and S. M. Saltiel. 10^{-10} temporal contrast for femtosecond ultraintense lasers by cross-polarized wave generation. *Opt. Lett.* **30**, 920 (2005)

[3] V. Chvykov, P. Rousseau, S. Reed, G. Kalinchenko, and V. Yanovsky. Generation of 10^{11} contrast 50 TW laser pulses. *Opt. Lett.* **31**, 1456 (2006)

[4] L. Canova, M. Merano, A. Jullien, G. Chériaux, R. Lopez-Martens, O. Albert, N. Forget, S. Kourtev, N. Minkovsky, and S. M. Saltiel. Coherent contrast improvement by cross-polarized wave generation. *I*n Conference on Lasers and Electro-Optics/Quantum Electronics and Laser Science Conference and Photonic Applications Systems Technologies **JThD131** (2007)

[5] M. Kalashnikov, K. Osvay, and W. Sandner. High-power Ti:Sapphire lasers: Temporal contrast and spectral narrowing. *Laser and Particle Beams* **25**, 219 (2007)

[6] M. P. Kalashnikov, K. Osvay, I. M. Lachko, H. Schönnagel, and W. Sandner. Suppression of gain narrowing in multi-tw lasers with negatively and positively chirped pulse amplification. *Appl. Phys. B*, **81**, 1059 (2005)

[7] T. Oksenhendler, D. Kaplan, P. Tournois, G. M. Greetham, and F. Estable. Intracavity acousto-optic programmable gain control for ultra-wide-band regenerative amplifiers. *Appl. Phys. B*, **83**, 491 (2006)

[8] H. Takada and K. Torizuka. Design and construction of a tw-class 12-fs ti:sapphire chirped-pulse amplification system. *Selected Topics in Quantum Electronics, IEEE Journal of*, **12**, 201 (2006)

[9] I. Pastirk, B. Resan, A. Fry, J. MacKay, and M. Dantus. No loss spectral phase correction and arbitrary phase shaping of regeneratively amplified femtosecond pulses using miips. *Optics Express*, **14**, 9537 (2006)

[10] A. Jullien, L. Canova, O. Albert, D. Boschetto, L. Antonucci, Y.-H. Cha, J. P. Rousseau, P. Chaudet, G. Chériaux, J. Etchepare, S. Kourtev, N. Minkovski, and S. M. Saltiel. Spectral broadening and pulse duration reduction during cross-polarized wave generation: influence of the quadratic spectral phase. *Appl. Phys. B* **87**, 595 (2007)

[11] M. P. Kalashnikov, E. Risse, H. Schönnagel, and W. Sandner. Double chirped-pulse-amplification laser: a way to clean pulses temporally. *Opt. Lett.* **30**, 923 (2005)

[12] M. E. Anderson, L. E. E. de Araujo, E. M. Kosik, and I. A. Walmsley. The effects of noise on ultrashort-optical-pulse measurement using spider. *Appl. Phys. B* **70**, S85 (2000)

[13] D. N. Fittinghoff, K. W. DeLong, R. Trebino, and C. L. Ladera. Noise sensitivity in frequency-resolved optical-gating measurements of ultrashort pulses. *J. Opt. Soc. Am. B* **12**, 1955 (1995)

[14] G. Stibenz, C. Ropers, C. Lienau, C. Warmuth, A. S. Wyatt, I. A. Walmsley, and G. Steinmeyer. Advanced methods for the characterization of few-cycle light pulses: a comparison. *Appl. Phys. B*, **83**, 511 (2006)

[15] E. Sidick, A. Dienes, and A. Knoesen. Ultrashort-pulse second-harmonic generation. non-transform-limited fundamental pulses. *J. Opt. Soc. Am. B* **12**, 1713 (1995)

[16] A. C. L. Boscheron, C. J. Sauteret, and A. Migus. Efficient broadband sum frequency based on controlled phase-modulated input fields: theory for 351-nm ultrabroadband or ultrashort-pulse generation. *J. Opt. Soc. Am. B*, **13**, 818 (1996)

[17] K. Osvay and I. N. Ross. Broadband sum-frequency generation by chirp-assisted group-velocity matching. *J. Opt. Soc. Am. B*, **13**, 1431 (1996)

[18] G. Veitas and R. Danielius. Generation of narrow-bandwidth tunable picosecond pulses by difference-frequency mixing of stretched pulses. *J. Opt. Soc. Am. B*, **16**, 1561 (1999)

[19] P. Baum, S. Lochbrunner, and E. Riedle. Generation of tunable 7-fs ultraviolet pulses: achromatic phase matching and chirp management. *Appl. Phys. B* **79**, 1027 (2004)

[20] C. Iaconis and I. A. Walmsley. Spectral phase interferometry for direct electric-field reconstruction of ultrashort optical pulses. *Opt. Lett.* **23**, 792 (1998)

[21] F. Verluise, V. Laude, Z. Cheng, Ch. Spielmann, and P. Tournois. Amplitude and phase control of ultrashort pulses by use of an acousto-optic programmable dispersive filter: pulse compression and shaping. *Opt. Lett.* **25**, 575 (2000)

4.9 XPW sub-10 fs pulses

4.9.1 Introduction

From the results presented in section 4.6 it is evident that, with correct control of the input spectral phase, the XPW pulses are not only spectrally broadened but also spectrally cleaned compared to the input pulses. Sub-10 fs pulses often present poor coherent temporal quality. A pedestal, whose relative intensity can reach 10^{-3} on a picosecond timescale, surrounds the main pulse [7, 8]. As discussed in section 2.2.2 degraded coherent contrast is partly due to imperfect compensation of high-order spectral phase, but also to strong modulations and sharp features of the spectral amplitude. This last characteristic is typical of ultra-broadband spectra generated through hollow-fiber and filamentation compression techniques [14, 22], or amplified in either saturated or non-saturated OPCPA stages. Even with ideal flat phase compression, modulated spectra lead to broad wings in the temporal domain [10]. It is therefore interesting to demonstrate the capability of XPW generation to clean the strong modulations of ultra-broad spectra. These experiments were done in collaboration with the former "Etudes des Lasers Femtosecondes" (ELF) group in LOA. The results are compared to the theoretical predictions presented in section 3.4.6.

4.9.2 Experimental setup and results

The experimental setup is shown in Fig. 4.17.

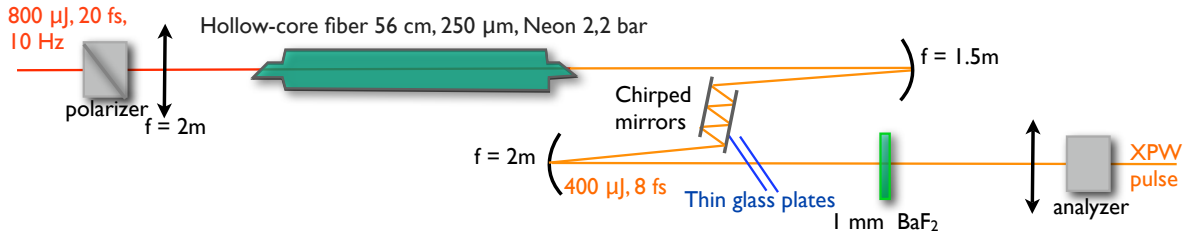

Figure 4.17: Experimental setup

The laser source is a Ti:Sa laser generating 1 mJ pulses, with a duration of 20 fs at 10 Hz repetition rate. To obtain pulse compression in the sub-10 fs range, 800 μJ pulses are focused to a hollow-core fiber (56 cm length, 250 μm inner diameter) filled with neon (2.2 bar) [14]. The transmission of the fiber is 50%. After propagation in the nonlinear medium, the spectrum is significantly broadened (600 nm - 950 nm) and exhibits strong modulations inherent to SPM and self-steepening processes (Fig. 4.18(a)). Chirped mirrors then provide adequate dispersion compensation($-200\,\mathrm{fs}^2$). A FROG measurement estimated the pulse duration to 8 fs (Fig. 4.18(b)) [15] which is close to the Fourier transform limit. These ultra-short pulses are sent in the XPW filter device, composed of one thin (1 mm) BaF_2 crystal ([101]) [16]) placed between crossed Glan polarizers. The first polarizer is placed at the entrance of the hollow fiber, where its intrinsic dispersion can be easily pre-compensated by the laser compressor adjustment. The

analyzer follows the nonlinear crystal to discriminate between the fundamental and XPW waves. The XPW filter contrast enhancement has been shown to be limited by the whole polarizing setup. We obtain 10^{-3} in our experiment. The BaF_2 crystal is placed close to the focus of a 2 m focal length mirror. When focused, the beam emerging as a single-mode from the hollow fiber presents an excellent spatial quality (Fig. 4.18(c)) which is favorable to get high XPW conversion efficiency. Moreover, the seeded energy of the 8 fs-pulses is reduced to 170 μJ to avoid additional nonlinear effects in air. This experiment is therefore a proof of principle.

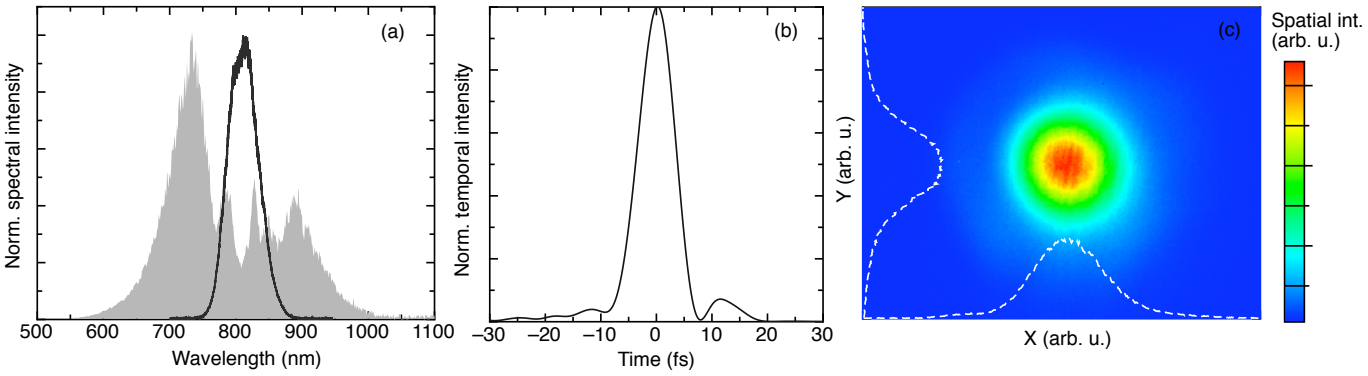

Figure 4.18: (a) Initial laser spectrum (black line) and spectrum measured after propagation in the hollow fiber (shaded area). (b) Pulse duration measurement after the hollow fiber by FROG technique (∼8 fs). (c) Spatial beam profile measured in the BaF_2 crystal plane (∼300 μm FWHM).

Filtering more energetic pulses would require the use of a vacuum or He-filled chamber. For such short pulses, one has to take into account the linear dispersion introduced by air and by the nonlinear crystal itself (380 fs^2/cm). For this reason, the chirp is over-compensated at the output of the fiber by two additional bounces on the chirped mirrors (total introduced dispersion:−300 fs^2). Thin BK7 plates (700 μm and a variable number of 150 μm plates) are inserted to optimize the degree of pulse compression for the XPW process.

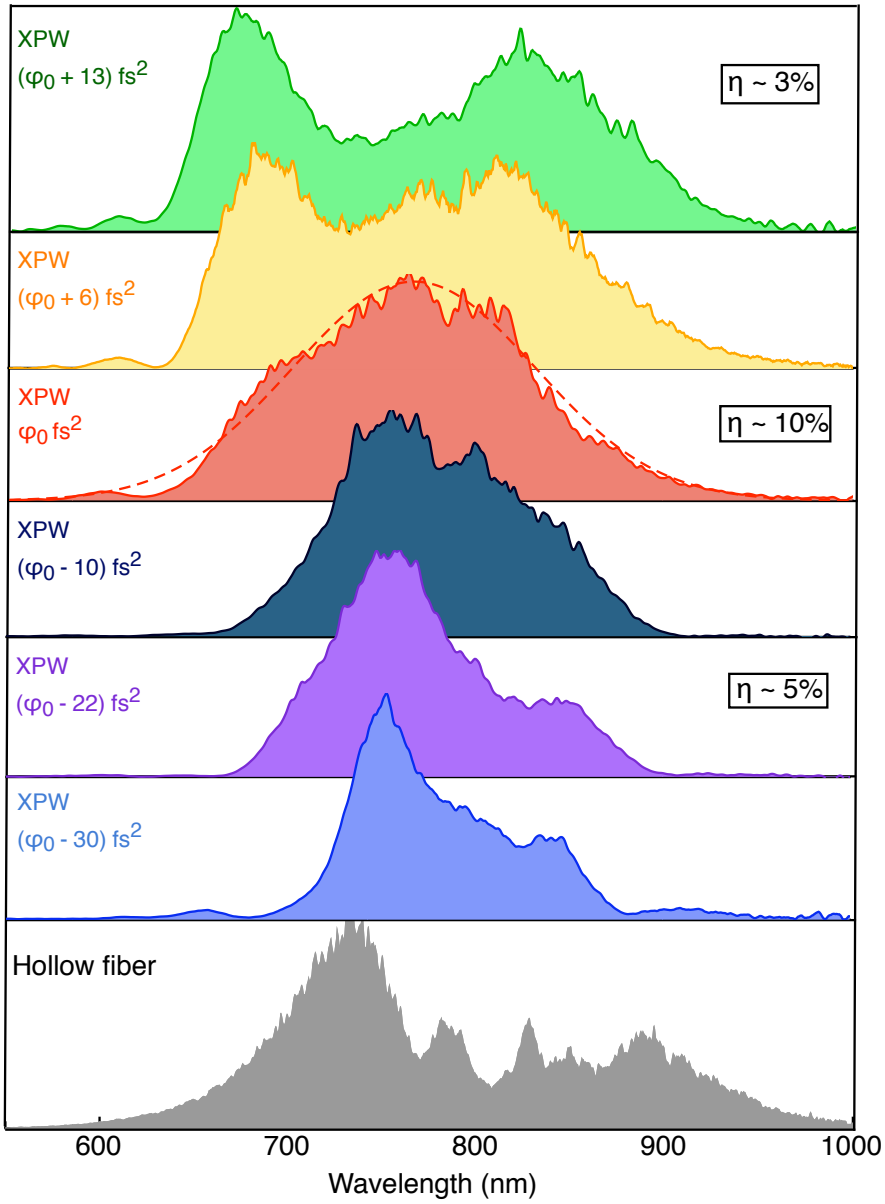

Figure 4.19: Experimental XPW spectra measured for various values of the residual chirp at the entrance of the crystal (values are relative to each other). The spectrum registered at the output of the hollow fiber is shown for comparison (grey area, lower panel). φ_0 is the residual input chirp, absolute value unknown, leading to the highest transmission efficiency of the process (10%) and providing a clean spectral quality. The corresponding output spectrum (red area) is fitted by a Gaussian shape (260 nm at $1/e^2$, dashed red line). The efficiency values are uncorrected from losses on the nonlinear crystal.

4.9.3 Analysis of the results

The experimental XPW spectral behavior as a function of residual second-order spectral phase is summarized in Fig. 4.19. The chirp compensation yielding the highest conversion efficiency is considered as the optimal pulse compression state accessible under our experimental conditions. The transmission of this single-crystal scheme is then slightly higher than 10% (uncorrected

for energy losses on the uncoated crystal faces). The residual input chirp in that case cannot be experimentally determined with accuracy and is simply labeled φ_0. The theoretical analysis presented in section 3.4.6 suggests that this residual input chirp corresponds to a slightly negative chirp ($-25f^2$). The optimized configuration also reveals the remarkable spectral cleaning effect of the process, as illustrated by the experimental output XPW spectrum plotted in Fig. 4.19 (XPW $\varphi_0\,\mathrm{fs}^2$). The input spectral bandwidth is preserved and the output spectrum has a smooth nearly-Gaussian shape. All the sharp features and fast modulations are eliminated.
XPW spectra registered for variable residual chirp (relatively to φ_0) at the entrance of the crystal show that the window for optimized compression is extremely narrow ($< 16\,\mathrm{fs}^2$, $\sim 40\,\mu$m of glass) (Fig. 4.19). They also show an asymmetry between the behavior for positive and negative input chirp. This asymmetry is correlated to the pulse dispersion during propagation in the crystal and was predicted theoretically in section 3.4.6. When the residual chirp is negative compared to φ_0, the available spectral bandwidth is narrower than that of the fundamental wave (Fig. 4.19 (XPW $(\varphi_0 - 10)\,\mathrm{fs}^2$, XPW $(\varphi_0 - 22)\,\mathrm{fs}^2$ and XPW $(\varphi_0 - 30)\,\mathrm{fs}^2$)), which is prohibitive. This is due to the fact that most of the conversion occurs with a negatively chirped pulse. The conversion efficiency in this regime is around 5%. On the other hand, if the residual chirp is positive compare to φ_0, the transmission becomes very weak (a few %). Despite being broader, the output spectrum is strongly modulated with sharp edges and a double-humped structure similar to the input spectrum (Fig. 4.19 (XPW $(\varphi_0 + 6)\,\mathrm{fs}^2$ and XPW $(\varphi_0 + 13)\,\mathrm{fs}^2$)). As predicted by the numerical simulations, in this case the conversion starts early in the crystal, and by the middle of the crystal the spectrum is very broad and smooth. Subsequent conversion takes place with a positively chirped pulse, leading to the evolution of a double humped output spectrum. These experimental results agree with the theory presented in section 3.4.6. We can then conclude that for this duration, (8 fs), the SVEA approximation is still acceptable.

4.9.4 Conclusion

With these experiments we have demonstrated the possibility of XPW filtering for sub-10 fs pulses. The energy conversion is acceptable for a single-crystal scheme (10%) and could be improved by using a two crystals configuration. We have also confirmed the influence of the dispersion in the non linear crystal. Very thin ($< 100\ \mu m$) or less dispersive (CaF_2, LiF) crystals are needed to generate spectrally cleaned and broadened XPW pulses.

Bibliography

[1] M. Hentschel, R. Kienberger, C. Spielmann, G. A. Reider, N. Milosevic, T. Brabec, P. Corkum, U. Heinzmann, M. Drescher, and F. Krausz, Attosecond metrology, Nature **414**, 509 (2001).

[2] M. Uiberacker, T. Uphues, M. Schultze, A. J. Verhoef, V. Yakovlev, M. F. Kling, J. Rauschenberger, N. M. Kabachnik, H. Schroder, M. Lezius, K. L. Kompa, H. G. Muller,

M. J. J. Vrakking, S. Hendel, U. Kleineberg, U. Heinzmann, M. Drescher, and F. Krausz, Supplementary information - attosecond real-time observation of electron tunnelling and multi-electron dynamics in atoms, Nature **446**, 627 (2007).

[3] C. Thaury, F. Quere, J. P. Geindre, A. Levy, T. Ceccotti, P. Monot, M. Bougeard, F. Reau, P. D'Oliveira, P. Audebert, R. Marjoribanks, and P. Martin, Plasma mirrors for ultrahigh-intensity optics, Nature Physics **3**, 424 (2007).

[4] G. D. Tsakiris, K. Eidmann, J. M. ter Vehn, and F. Krausz, Route to intense single attosecond pulses, New Journal of Physics **8** (2006).

[5] N. M. Naumova, C. P. Hauri, J. A. Nees, I. V. Sokolov, R. Lopez-Martens, and G. A. Mourou, Towards efficient generation of attosecond pulses from overdense plasma targets, New Journal of Physics **10**, 025,022 (2008).

[6] F. Tavella, A. Marcinkevicius, and F. Krausz, Investigation of the superfluorescence and signal amplification in an ultrabroadband multiterawatt optical parametric chirped pulse amplifier system, New Journal of Physics **8**, 219 (2006).

[7] F. Tavella, K. Schmid, N. Ishii, A. Marcinkevicius, l. Veisz, and F. Krausz, High-dynamic range pulse-contrast measurements of a broadband optical parametric chirped-pulse amplifier, Applied Physics B **81**, 753–756 (2005).

[8] N. Forget, A. Cotel, E. Brambrink, P. Audebert, C. L. Blanc, A. Jullien, O. Albert, and G. Chériaux, Pump-noise transfer in optical parametric chirped-pulse amplification, Optics Letters **30**, 2921–2923 (2005).

[9] C. Dorrer and J. Bromage, Impact of high-frequency spectral phase modulation on the temporal profile of short optical pulses, Opt. Express **16** (2008).

[10] K. Osvay, M. Csatari, I. N. Ross, A. Persson, and C. G. Wahlstrom, On the temporal contrast of high intensity femtosecond laser pulses, Lasers and Particle Beams **23**, 327 (2005).

[11] A. Jullien, O. Albert, F. Burgy, G. Hamoniaux, J.-P. Rousseau, J.-P. Chambaret, F. Augé-Rochereau, G. Chériaux, J. Etchepare, N. Minkovski, and S. M. Saltiel, 10^{-10} temporal contrast for femtosecond ultraintense lasers by cross-polarized wave generation, Opt. Lett. **30**, 920–922 (2005).

[12] A. Jullien, O. Albert, G. Chériaux, J. Etchepare, S. Kourtev, N. Minkovski, and S. M. Saltiel, Highly efficient temporal cleaner for femtosecond pulses based on cross-polarized wave generation in a dual crystal scheme, App. Phys. B **84**, 409–414 (2006).

[13] V. Chvykov, P. Rousseau, S. Reed, G. Kalinchenko, and V. Yanovsky, Generation of 10^{11} contrast 50 TW laser pulses, Opt. Lett. **31**, 1456–1458 (2006).

[14] M. Nisoli, S. D. Silvestri, and O. Svelto, Generation of high energy 10 fs pulses by a new pulse compression technique, Appl. Phys. Lett. **68**, 2793 (1996).

[15] S. Akturk, C. D'Amico, and A. Mysyrowicz, Measuring ultrashort pulses in the single-cycle regime using frequency-resolved optical gating, J. Opt. Soc. Am. B **25**, A63 (2008).

[16] L. Canova, S. Kourtev, N. Minkovski, A. Jullien, R. B. Lopez-Martens, O. Albert, and S. M. Saltiel, Efficient generation of cross-polarized femtosecond pulses in cubic crystals with holographic cut orientation, Appl. Phys. Lett. **92**, 231,102 (2008).

[17] F. Tavella, Y. Nomura, L. Veisz, V. Pervak, A. Marcinkevicius, and F. Krausz, Dispersion management for a sub-10-fs, 10 tw optical parametric chirped-pulse amplifier, Optics Letters **32**, 2227 (2007).

[18] H. Wang, Y. Wu, C. Li, H. Mashiko, S. Gilbertson, and Z. Chang, Generation of 0.5 mj, few-cycle laser pulses by an adaptive phase modulator, Opt. Express **16**, 14,448–14,455 (2008).

[19] A. Jullien, L. Canova, O. Albert, D. Boschetto, L. Antonucci, Y.-H. Cha, J. P. Rousseau, P. Chaudet, G. Cheriaux, J. Etchepare, S. Kourtev, N. Minkovski, and S. M. Saltiel, Spectral broadening and pulse duration reduction during cross-polarized wave generation: influence of the quadratic spectral phase, App. Phys. B **87**, 595 (2007).

[20] L. Canova, O. Albert, N. Forget, B. Mercier, S. Kourtev, N. Minkovski, S. M. Saltiel, and R. Lopez-Martens, Influence of spectral phase on cross-polarized wave generation with short femtosecond pulses, App. Phys. B (2008).

[21] A. Jullien, O. Albert, G. Cheriaux, J. Etchepare, S. Kourtev, N. Minkovski, and S. M. Saltiel, A two crystal arrangement to fight efficiency saturation in cross-polarized wave generation, Opt. Express **14**, 2760–2769 (2006).

[22] C.P. Hauri, W. Kornelis, F.W. Helbing, A. Heinrich, A. Couairon, A. Mysyrowicz, J. Biegert, and U. Keller. Generation of intense, carrier-envelope phase-locked few-cycle laser pulses through filamentation. *Applied Physics B: Lasers and Optics*, 79(6):673–677, October 2004.

4.10 XPW in UV

In all previous sections XPW generation has been studied in the visible/infrared region. In this section, I present an experimental investigation of the efficiency of XPW generation in the near UV region. These experiments have been done in collaboration with S. Kourtev and N. Minkowki from the Sofia University "St. Kliment Ohridski" (Bulgaria).

There are several motivations to extend the XPW process to shorter wavelength:
first femtosecond excimer laser amplifiers are being developed as ultra-intense femtosecond UV laser sources and they could be advantageous in many applications (material processing, biomedicine, laser fusion, etc.). Contrast improvement of these sources is of importance since ASE in the UV is directly absorbed during laser–matter interaction. Avoiding pre–plasma formation requires the ASE level in the UV region to be kept even lower than in the infrared.
Second XPW generation can be used as the nonlinear effect in diagnostics for the characterization of UV short pulses (section 2.3.4). It complies with the requirements of a useable nonlinear effect: it is efficient, achromatic, presents intrinsic phase matching, generates a measurable signal wavelength (identical to the input one) easily discriminated from the input pulses through its polarization. So it should be compared to several other methods used to measure the temporal profile or the temporal contrast of UV pulses (two-photon fluorescence in alkali-earth fluoride crystals [6, 7], self-diffraction or cross-phase modulation). A first demonstration of an XPW FROG in the visible (400nm) is reported in [8].
The last motivation is that few-cycle pulses consist of an ultra-broad spectrum spanning from the IR down to the U.V. Until now I have always assumed that the $\chi^{(3)}$ tensor is constant with wavelength. This is not verified anymore for photon energies approaching half the crystal band-gap. In this section, I present an experimental investigation of the efficiency of XPW generation in the near UV region (310 nm). By comparing XPW efficiency at 310 and 620 nm an estimate of the dispersion of $\chi^{(3)}$ in BaF_2 is obtained.

4.10.1 Experimental setup

The experimental setup is shown in Fig. 4.20. The pumping source is a CPM dye laser frequency-doubled in a 3 mm type I KDP crystal ($\lambda = 310$ nm after the doubling, $\tau \approx 100$ fs, repetition rate 10 Hz). The pulses are focused (f = 300 mm) into a 2 mm z-cut BaF_2 crystal placed between crossed, high extinction ratio, calcite UV grade polarizers (transparency range 0.22-2.3 μm). BaF_2 is highly transparent in the UV as it presents a cut-off at 150 nm and the losses due to two-photon absorption (TPA) are small (Fig. 4.21). To compare XPW generation in the UV with XPW generation behavior in the visible, measurements are also performed at the fundamental laser wavelength $\lambda = 620$ nm by removing the KDP doubling crystal and UV filter and using a focal length of 450 mm.

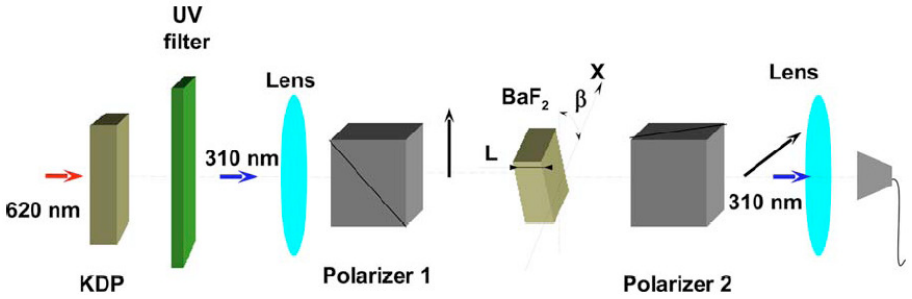

Figure 4.20: Schematic of the XPW experiment in UV region. BaF_2 it's a z-cut sample. β is the angle between the x-axis of the crystal and the polarization plane of the input beam.

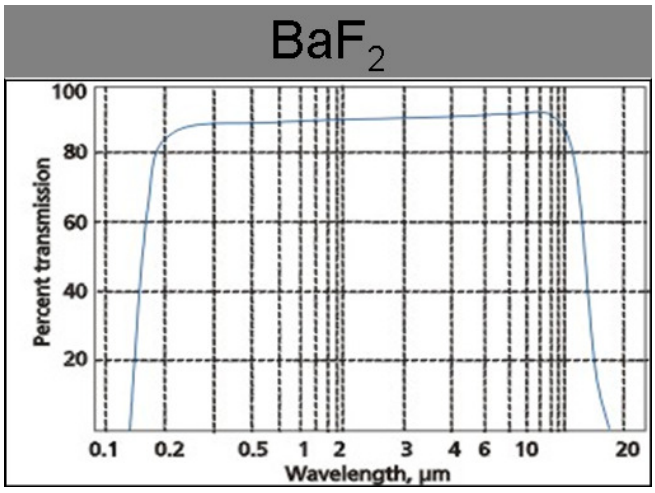

Figure 4.21: Transmission of BaF_2 crystal function of the wavelength λ (Saint-Gobain.)

4.10.2 Experimental results

XPW experiments in the UV immediately prove that XPW generation is not only possible at those wavelength but also that it is more efficient than in visible. To quantify the increase in XPW generation efficiency in the UV we did two type of experiments. We measured, both in the UV and the visible, the XPW intensity as a function of input intensity and crystal orientation. This gives two independent methods to measure the efficiency increase in the UV, which can then be compared to a theoretical model.

XPW generation efficiency measurements as a function of input intensities and wavelength are presented in Fig. 4.22. To estimate the input intensity, the spot surfaces of the input beams

(UV and VIS) were carefully measured. The ratio of spot surfaces (VIS/UV) was found to be 2.17 . Furthermore, the pulse durations were found to be identical for both wavelengths due to second harmonic generation (SHG) experimental conditions. The KDP crystal thickness is such that the difference in group velocities causes narrowing of the SHG spectrum that counterparts the $\sqrt{2}$ broadening due to the SHG process.

The slope of the XPW generation efficiency as a function of the input pulse intensity follows a quadratic law as it should be for any cubic nonlinear process. For a given input intensity, XPW efficiency is 6 times higher in UV than in visible when XPW generation is unsaturated. As seen from Fig. 4.22 in the saturation regime, XPW efficiency is the same in the visible and in the UV.

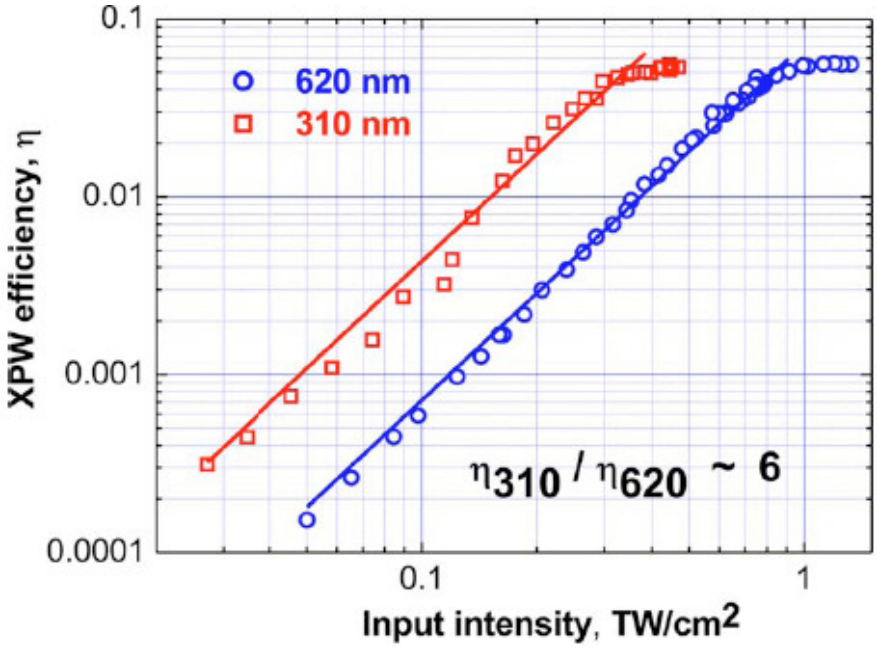

Figure 4.22: Comparison of XPW efficiencies at 310 nm and 620 nm. The solid lines represents quadratic dependence.

XPW efficiency being linked to $\chi^{(3)}$ anisotropy, it is strongly dependant on crystal axes orientation with respect to the input pulse polarization. The measured angular dependence of the XPW efficiency at λ=310 nm and λ=620 nm (pulse energies of 15.5 μJ and 56 μJ respectively) are presented in Fig. 4.23. β is the angle between the input polarization plane and the crystal axis x. The two energies correspond to intensities of 465 GW/cm^2 $\pm$ 10% at 310 nm and to 780 GW/cm^2 $\pm$ 10% at 620 nm, respectively.

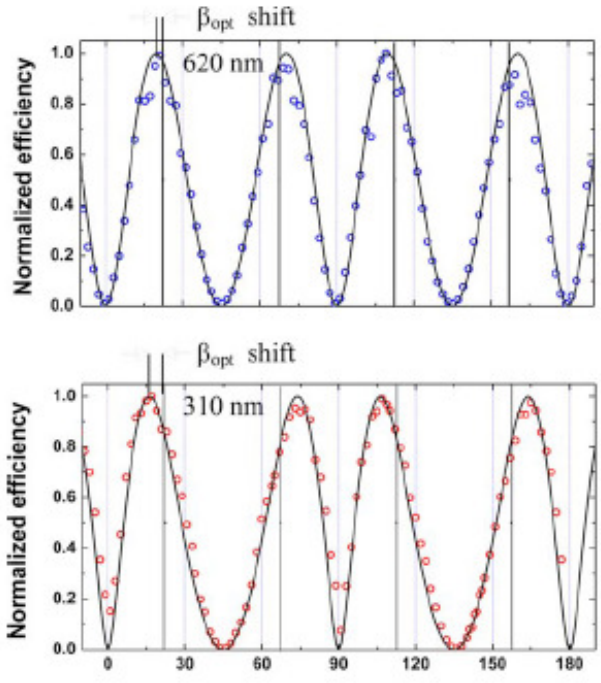

Figure 4.23: XPW generation efficiency as a function of angle β for (a) 620 nm and (b) 310 nm fundamental wavelengths. Each of the experimental curves is normalized to the average value of the maxima. The lines are theoretical curves for Gauss/Gauss shapes for spatial/temporal modulation of the fundamental radiation for (a) F=3.6 and (b) F=5.76. The theoretical model used takes into account SPM and depletion of the fundamental wave. The vertical solid lines indicate optimal β position for low input intensities when $F << 1$

4.10.3 Analysis of the results

From the results shown on Fig. 4.22 and 4.23 we can estimate the increase in third order nonlinearity at 310 nm with respect to 620 nm. In the undepleted regime the XPW efficiency η is given by:

$$\eta = \frac{I_{XPW}}{I_0} = \frac{2}{\epsilon_o cn}[(\sigma/4)\gamma_o I_o sin(4\beta)L]^2 \tag{4.3}$$

where I_0 is input intensity, $\gamma_0 = 6\pi\chi^{(3)}_{xxxx}/8n\lambda$; L is the crystal length; σ is the anisotropy of $\chi^{(3)}$ -tensor $\sigma = (\chi^{(3)}_{xxxx} - 3\chi^{(3)}_{xxyy})/\chi^{(3)}_{xxxx}$. Therefore, η varies with λ for two reasons. First it presents a $1/\lambda^2$ dependance due to the dispersion of γ_0. Second it is sensitive to the dispersion of $\chi^{(3)}$. As there is no data on the dispersion of σ we are able to measure the dispersion of $|\sigma\chi^{(3)}_{xxxx}|$ and assume that the dispersion of σ is negligible compare to the dispersion of $\chi^{(3)}$.

From measurements presented in Fig. 4.22, and using Eq. (4.3), we obtain a value of $|\sigma\chi^{(3)|}_{xxxx}$ which is 1.22 times higher at 310 nm than at 620 nm.

This is confirmed by the β scan analysis. XPW generation with high efficiency presents a β dependency that varies with $F = (2/\epsilon_o cn)\sigma\gamma_o I_o L$. The F parameter is the S parameter already defined multiplied by the anisotropy. When $F << 1$ the position of the maxima are at $\beta_{opt} = m.22.5^o$ with m integer. These positions are marked with vertical solid lines in Fig. 4.23.

At higher values of F the maxima are shifted from the low intensity positions. The bigger is the F parameter the bigger is the shift of β_{opt} from its low intensity position. Using F as a fitting parameter theoretical dependencies are plotted on Fig. 4.23. The corresponding F fitting parameters for both β experimental curves are $F_{620} = 3.6$ for the 620 nm experiment and $F_{310} = 5.76$ for the 310 nm experiment. Using the ratio $F_{310}/F_{620} = 1.60$ and the ratio $I_{o,310}/I_{o,620} = 0.60$ we obtain that the product $|\sigma(\chi^{(3)}_{xxxx}|$ is 1.33 times higher at 310 nm than that at 620 nm.

The main source of error in both intensity and beta dependence measurements is the input intensity measurement uncertainty. We then may conclude that the two estimations for the ratio $(\sigma\chi^{(3)}_{xxxx})_{310}/(\sigma\chi^{(3)}_{xxxx})_{620}$ are in accordance with each other giving an overall:

$$\sigma\chi^{(3)}_{xxxx})_{310}/(\sigma\chi^{(3)}_{xxxx})_{620} = 1.28 \pm 0.10 \tag{4.4}$$

$\chi^{(3)}_{xxxx}$ dispersion of BaF_2 as a function of the wavelength has been previously experimentally investigated by De-Salvo et al [9] using a Z-scan measurement at 1064 nm, 532 nm, 355 nm and 266 nm. Interpolating data in ref [9] one can estimate $\kappa = (\chi^{(3)}_{xxxx})_{310}/(\chi^{(3)}_{xxxx})_{620} \approx 1.4$. This ratio is comparable to the one reported in this section. Furthermore, we can also conclude that the dispersion of σ, the anisotropy of $\chi^{(3)}$, in the spectral range investigated is small and does not exceed the dispersion of $\chi^{(3)}_{xxxx}$.

Theoretical model

The method of Boling-Glass-Owyoung [10] is frequently used to theoretically derive the cubic nonlinearities of materials from their optical index. Furthermore, using the Sellmeier equation for optical index dispersion with this model, the dispersion of $\chi^{(3)}_{xxxx}$ for BaF_2 is given by:

$$\chi^{(3)}_{xxxx}(\lambda) = \chi^{(3)}_{xxxx}(\lambda_o)\frac{n(\lambda)[n(\lambda)^2+2]^2[n(\lambda)^2-1]^2}{n(\lambda_o)[n(\lambda_o)^2+2]^2[n(\lambda_o)^2-1]^2} \tag{4.5}$$

Applying this equation (4.5) to the wavelengths relevant to this experiment we obtain $\kappa = (\chi^{(3)}_{xxxx})_{310}/(\chi^{(3)}_{xxxx})_{620} \approx 1.17 \pm 0.20$ This estimation is also consistent with the measured value from this section enforcing the hypothesis that σ presents little dispersion with wavelength.

4.10.4 Conclusion

In conclusion, with these experiments we have demonstrated XPW generation in UV region and that this process, outside saturation, is 6 times more efficient than in the visible. Efficiency dependence with input wavelength from λ_o to λ, in the visible and near UV region, can be described by the following relation:

$$\eta(\lambda) = \eta(\lambda_o)(\kappa\frac{\lambda_o}{\lambda})^2 \tag{4.6}$$

The value reported here for κ is in accordance with what has been previously reported. The results presented here will be useful for extending the XPW nonlinear filter in the UV region and

for developing new applications as, for example, pulse characterization and temporal contrast filtering of femtosecond UV pulses. Similar results obtained with LiF crystal at 310 nm shows that XPW can be extended to wavelength as low as 266 nm (cut-off frequency at 100 nm).

Bibliography

[1] A. Jullien, O. Albert, F. Burgy, G. Hamoniaux, J.- P. Rousseau, J.-P. Chambaret, F. Auge-Rochereau, G. Cheriaux, J. Etchepare, N. Minkovski, and S. Saltiel. 10^{-10} temporal contrast for femtosecond ultraintense lasers by cross-polarized wave generation. *Opt. Lett.* **30**, 920-922 (2005).

[2] V. Chvykov, P. Rousseau, S. Reed, G. Kalinchenko, and V. Yanovsky. Generation of 10^{11} contrast 50 TW laser pulses. *Opt. Lett.* **31**, 1456 (2006)

[3] S. S. Bulanov, A. Brantov, V. Yu. Bychenkov, V. Chvykov, G. Kalinchenko, T. Matsuoka, P. Rousseau, S. Reed, V. Yanovsky, K. Krushelnick, D. W. Litzenberg and A. Maksimchuk. Accelerating protons to therapeutic energies with ultra-intense ultra-clean and ultra-short laser pulses. *Med. Phys.* **35**, 1770 (2008).

[4] A. Cotel, A. Jullien, N. Forget, O. Albert, G. Ch´eriaux, C.L. Blanc, Appl. Phys. B **83**, 7 (2006).

[5] N. Minkovski, G. I. Petrov, S. M. Saltiel, O. Albert, and J. Etchepare. Nonlinear polarization rotation and orthogonal polarization generation experienced in a single-beam configuration. *J. Opt. Soc. Am. B* **21**, 1659 (2004

[6] K. Osvay, I.N. Ross, C.J. Hooker, J.M.D. Lister. Laser-excited nonlinear properties of BaF_2 and its application in a single-shot spatially insensitive autocorrelator. *Appl. Phys.* B 59, 361 (1994).

[7] K. Osvay, M. Csataria, A. Gaal and I. N. Ross. Temporal Contrast of High Intensity Femtosecond UV Pulses. *Journal of the Chinese Chemical Society* 47, 855 (2000).

[8] N. Forget, S. Coudreau, F. Lepetit, O. Albert, T. Oksenhendler. Achromatic and Single-beam Pulse Characterization Technique for Visible-UV Pulses based on direct UV Pulse Shaping and Cross- polarized Wave Generation. *Lasers and Electro-Optics*, 2007. CLEO 2007.Page(s):1 - 2,CMA3.

[9] R. DeSalvo, A. A. Said, D. J. Hagan, E.W. Van Stryland, M. Sheik-Bahae,"Infrared to ultraviolet measurements of two-photon absorption and n_2 in wide bandgap solids. *IEEE Journal of Quantum Electronics* 32, 1324 - 1333 (1996).

[10] N. Boling, A. Glass, A. Owyoung. Empirical relationships for predicting nonlinear refractive index changes in optical solids. *IEEE Journal of Quantum Electronics*, 14, 601 (1978).

4.11 High energy XPW

4.11.1 Introduction

I have previously shown that, working in a double, holo-cut crystal configuration, XPW generation efficiency close to 30 % in energy can be reached (Fig. 4.7). In this configuration the first crystal is placed in the far field (at the focus) to have a good spatial profile and the position of the second crystal is optimized to maximize the overall efficiency. With this solution we obtained 55 μJ for an input energy of 190 μJ.
Today the most common front-ends of high intensity laser systems deliver mJ level, $\approx$ 30 fs pulses. This is for example the case of the LOASIS laser system presented in chapter 5 and of the "salle noire" laser system (the front-end is a commercial Femtopower CEP from Femtolasers GmbH) presented in chapter 6. The Femtopower system is also used as the front-end of the 100 TW laser system produced by Thales Laser (Alpha 10). The only solution at the moment, for implementing an XPW filter after the front-end is to decrease the input pulse energy. The consequence is that only several tens of μJ of XPW signal are obtained and an additional booster stage may be necessary before injecting into the low gain amplifiers. Furthermore, with the constant increase in focused intensity on target (PetaWatt class lasers), pulses with a temporal contrast higher than 10 orders of magnitude are needed. This implies injecting > 100 μJ, ultra high contrast pulses into the second CPA. There is therefore a big interest in trying to extend the high efficiency demonstrated at the hundreds of μJ level to higher input energy and, in particular, to the mJ level.
Several difficulties limit this extension. First, working in the far field and increasing the input energy (keeping the intensity on the crystal below the white-light generation threshold ($10^{12} W/cm^2$)), implies using very long focal lengths. The focal length for filtering 200 μJ, with an input beam diameter of 7 mm, is already 4 meters. The second problem is linked to the two-crystal configuration. Fig. 4.24 shows the optimal distance between the two crystals as a function of the focal length squared. The input beam diameter is 5 mm. The distance between the crystals increases linearly with the square of focal length and so with the input energy.

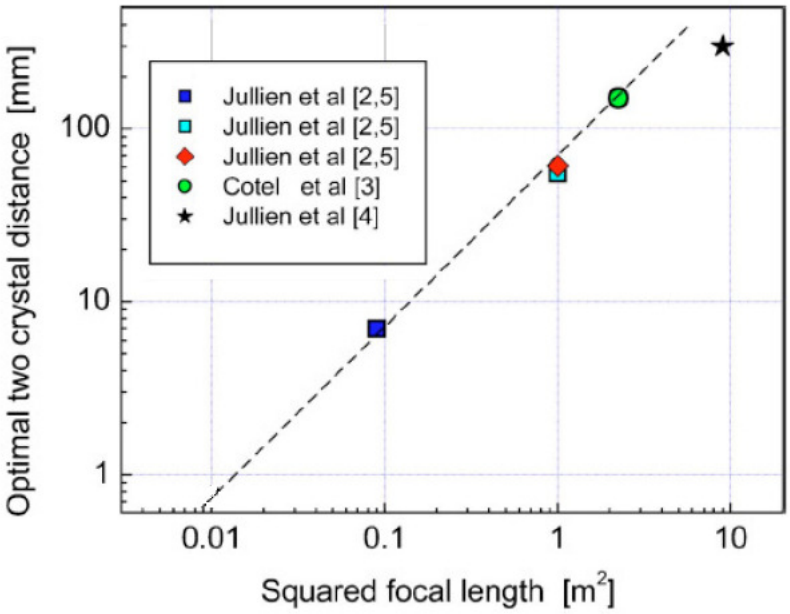

Figure 4.24: Summary of published optimal distances with two crystal schemes for XPW generation obtained with different focusing of the fundamental beam on the two crystal setup. The dashed lines corresponds to the theoretically predicted slope of 1.

Just as an example, in order to filter 1 mJ, 30 fs pulses, in the double crystal configuration, the second crystal needs to the located at more than 1 meter from the first. This also implies that several meters of propagation need to be put under vacuum to avoid any temporal and spatial distortion caused by SPM. These distances can be reduced by entering with a smaller beam size but this complicates the beam propagation and implies re-expanding the beam to avoid damaging the output polarizer.
The simplest solution to bypass these scaling effects consists in using a relatively short focal length (for example 1 m) and putting the crystal in the near field (out of focus). To circumvent the problem of poor spatial quality in the near field, a hard aperture can be placed in the focus to act as a spatial filter. The first results with this configuration were obtained after the-front end of a commercial 200 TW laser system (Amplitude Technologies) and are presented in the next section. This type of front-end was chosen because, thanks to the amplification in a regenerative amplifier, the M^2 is very close to 1 and the good spatial profile is maintained out of focus. Furthermore pulses with an energy higher than 10 mJ are available. With a conversion efficiency of 10 % in a single crystal configuration, XPW pulses approaching the 1 mJ level can be expected. This also makes it possible to measure, with high dynamic range, the temporal contrast directly after the XPW filter.

4.11.2 Experiments at Amplitude Technologies

The 200 TW Pulsar laser system (from Amplitude Technologies, France) is a CPA femtosecond laser source providing more than 5 J pulse energy at 10Hz repetition rate, with a peak power of 200 TW. It consists of a fully integrated Ti:Sa oscillator with a diode pumped solid state pump

laser, a stretcher, a regenerative amplifier, three multi-pass amplifiers pumped by Nd:YAG lasers and a vacuum compressor. The experiments described here were performed using the front-end only, limiting the energy and allowing pulse compression in air. With the gain narrowing control performed with an Acousto-Optic Programmable Gain Control Filter (AOPGCF, Mazzler) [2], spectra as wide as 80 nm are typically generated, only limited by the stretcher and mirrors bandpass. Due to the square shape of those spectra, the corresponding measured pulse durations is < 25 fs. The system overall spectral phase is carefully and actively controlled using a feedback loop between a spectral phase retrieval device, a commercial APE Spider, and the Dazzler. Using this technique, deviations from a flat spectral phase of less than 0.5 rad are achievable over about 100 nm spectral range.

To test the new XPW configuration the $\approx 25fs$, multi-mJ pulses, compressed after the front-end, pass through a variable neutral density filter for energy tuning and are focused with a 1 meter focal lens onto a 300 μm iris. The focal spot matches the sizes of the iris. A single BaF_2 1 mm, [101]-cut crystal is placed after the focus at a correct distance to stay just below the white-light generation threshold. The iris and the crystal are placed under vacuum in a plexiglass tube (Fig. 4.25). The transverse position of the iris and the longitudinal position of the crystal can be optimized by keeping the system under vacuum. The position of the single crystal is optimized to saturate the XPW effect without distortion of the spectrum. The generated XPW beam is selected with a, high extinction ratio, calcite Glan polarizer. The maximum output XPW energy we obtained is $\approx$ 1 mJ for an input of 10 mJ yielding an overall efficiency of 10 % (considering the losses through the iris) and a good spatial quality. The measured spectrum (Fig. 4.27 black line) is well fitted by a Gaussian and has a FWHM larger than 100 nm corresponding to sub-10 fs Fourier transform pulses. The actual temporal duration is $>$ 100 fs due to the dispersion (550 fs^2) added by the output Glan polarizer. This dispersion can be compensated with multiple bounces on broadband chirped mirrors. These mirrors were not available for the current experiment. The XPW spectrum is broadened and not shifted compared to the fundamental. As explained in section 4.6 this is an indication of the good compression of the input beam. The XPW energy stability function of time is shown in Fig. 4.26 while Fig. 4.28(black line) shows the high dynamic temporal contrast of the filtered pulses measured with a third order correlator (Sequoia, Amplitude Technologies). The dispersion added by the output window of the vacuum tube and the thick Glan polarizer is not compensated. The Sequoia measurement dynamic range is close to 12 orders of magnitude for a 1 mJ input pulse. To make the increase in temporal contrast clearly visible we started with the laser with a low temporal contrast ($< 10^5$ red line). An increase in temporal contrast of 5 orders magnitude is visible in the ns (ASE) and ps (coherent contrast) zone. This enhancement is determined by the ratio between the two components of the input linear polarization. These experiments confirm the resulted presented in [1] but with a scaling of the output energy by almost a factor 10.

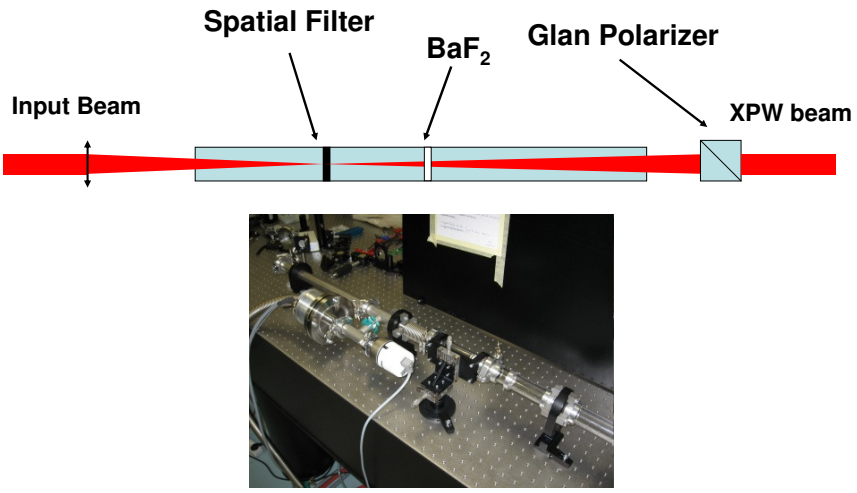

Figure 4.25: Schematic of the setup. An iris is placed in the focus to act as a spatial filter. The position of the crystal is optimized to have a good efficiency without distortion of the generated XPW spectrum. A maximum output energy of 850 μJ has been obtained.

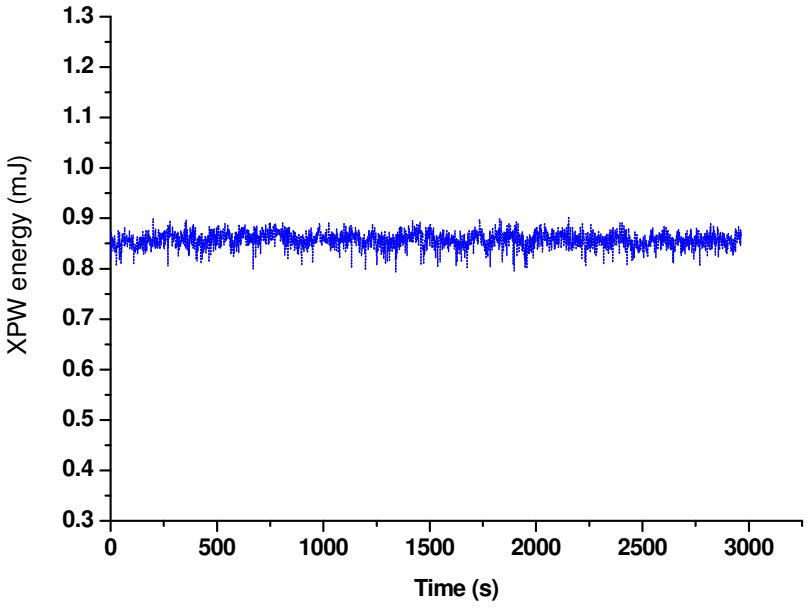

Figure 4.26: Energy of the XPW pulses function of time

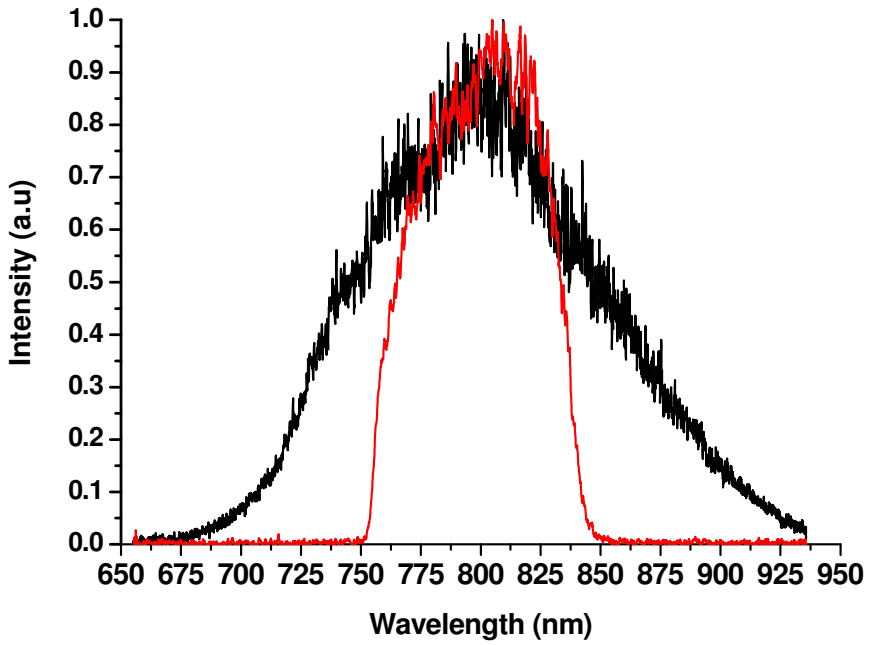

Figure 4.27: Spectrum of the converted XPW pulses(black line) and of the fundamental (red line)

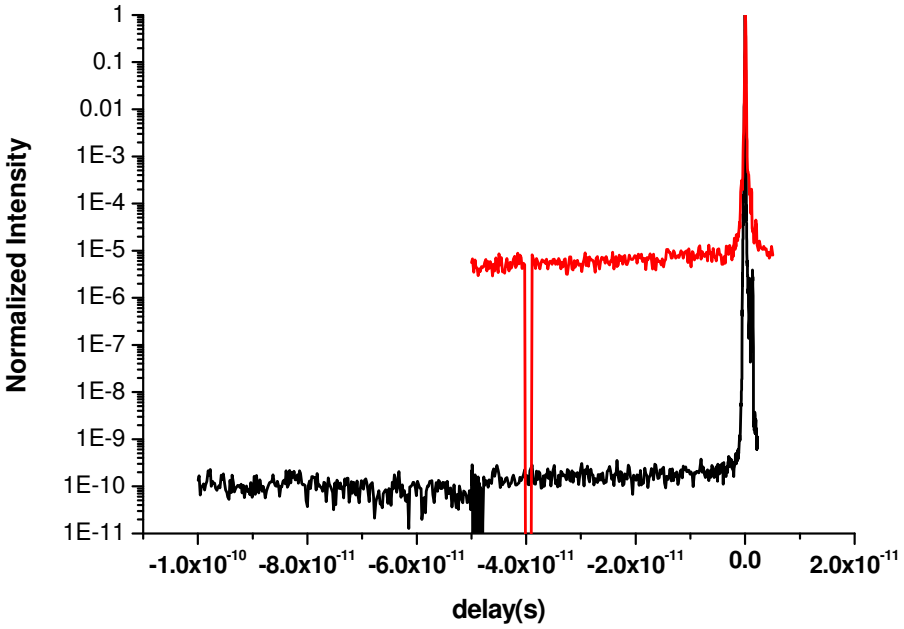

Figure 4.28: Third order correlator (Sequoia, Amplitude Technologies) measurement of the temporal contrast of initial laser (red line) and after the XPW filter (black line). The energy of the XPW beam was 850 μJ

4.11.3 Conclusion

In conclusion the results of these preliminary experiments are very promising. The possibility of obtaining 1 mJ, spectrally cleaned and broadened pulses was demonstrated. Starting with high contrast input pulses (10^{10} for a typical Amplitude Technologies system) opens the possibility for generating sub-20 fs pulses with a temporal contrast higher than 14 orders of magnitude.

Bibliography

[1] A. Jullien, O. Albert, F. Burgy, G. Hamoniaux, J.-P. Rousseau, J.-P. Chambaret, F. Augé-Rochereau, G. Chériaux, J. Etchepare, N. Minkovski, and S. M. Saltiel. 10^{-10} temporal contrast for femtosecond ultraintense lasers by cross-polarized wave generation. *Opt. Lett.*, 30(8):920–922, 2005.

[2] T. Oksenhendler, D. Kaplan, P. Tournois, G.M. Greetham, and F. Estable. Intracavity acousto-optic programmable gain control for ultra-wide-band regenerative amplifiers. *Applied Physics B: Lasers and Optics*, 83(4):491–494, June 2006.